Cerebral Cortex, February 2017;27: 933–949

doi: 10.1093/cercor/bhx016
Advance Access Publication Date: 3 February 2017
Original Article

ORIGINAL ARTICLE

Reduced Inhibition within Layer IV of *Sert* Knockout Rat Barrel Cortex is Associated with Faster Sensory Integration

Stéphanie Miceli[1,2], Nael Nadif Kasri[1,3], Joep Joosten[1], Chao Huang[4], Lara Kepser[1], Rémi Proville[4], Martijn M. Selten[1], Fenneke van Eijs[1], Alireza Azarfar[4], Judith R. Homberg[1], Tansu Celikel[4] and Dirk Schubert[1,4]

[1]Department of Cognitive Neuroscience, Radboudumc, Donders Institute for Brain, Cognition and Behaviour, Nijmegen, The Netherlands, [2]Department of Neural Networks, Center of Advanced European Studies and Research (caesar), Max Planck Society, Germany, [3]Department of Human Genetics, Radboudumc, Donders Institute for Brain, Cognition and Behaviour, Nijmegen, The Netherlands and [4]Department of Neurophysiology, Donders Institute for Brain, Cognition and Behaviour, Radboud University, Nijmegen, The Netherlands

Address correspondence to Dr Dirk Schubert, P.O. Box 9101, 6500 HB Nijmegen, The Netherlands. Email: d.schubert@donders.ru.nl

Abstract

Neural activity is essential for the maturation of sensory systems. In the rodent primary somatosensory cortex (S1), high extracellular serotonin (5-HT) levels during development impair neural transmission between the thalamus and cortical input layer IV (LIV). Rodent models of impaired 5-HT transporter (SERT) function show disruption in their topological organization of S1 and in the expression of activity-regulated genes essential for inhibitory cortical network formation. It remains unclear how such alterations affect the sensory information processing within cortical LIV. Using serotonin transporter knockout (*Sert*$^{-/-}$) rats, we demonstrate that high extracellular serotonin levels are associated with impaired feedforward inhibition (FFI), fewer perisomatic inhibitory synapses, a depolarized GABA reversal potential and reduced expression of KCC2 transporters in juvenile animals. At the neural population level, reduced FFI increases the excitatory drive originating from LIV, facilitating evoked representations in the supragranular layers II/III. The behavioral consequence of these changes in network excitability is faster integration of the sensory information during whisker-based tactile navigation, as *Sert*$^{-/-}$ rats require fewer whisker contacts with tactile targets and perform object localization with faster reaction times. These results highlight the association of serotonergic homeostasis with formation and excitability of sensory cortical networks, and consequently with sensory perception.

Key words: 5-HT, 5-HTT, feedforward inhibition, serotonin, somatosensory

Introduction

Sensory experience and neuronal activity collectively drive the development of inhibitory cortical circuitry (Huang 2009), starting during the second postnatal week in the rodent neocortex (Luhmann and Prince 1991; Daw et al. 2007; Huang 2009; Zhang et al. 2011; Le Magueresse and Monyer 2013). During this

initial critical period for the inhibitory cortical circuitry, sensory deprivation, which leads to reduced neural transmission between the thalamus and sensory cortex, has been associated with an impaired maturation of inhibitory synapses (Kilman et al. 2002; Hensch 2005; Gao et al. 2014), lower inhibitory drive (Chamma et al. 2012), deficits in feedforward inhibitory mechanisms (Chittajallu and Isaac 2010) as well as altered excitatory and inhibitory receptive field maturation within cortical layer IV (LIV) (Shoykhet et al. 2005).

Rodents exposed to elevated brain serotonin (5-HT) levels early in development represent useful models to investigate the effects of such reduced afferent activity at the thalamocortical (TC) synapse. During the first postnatal weeks, 5-HT1B receptor activation on TC synapses impairs the probability of glutamate release onto neurons within the main input LIV of the somatosensory cortex (Rhoades et al. 1994; Laurent et al. 2002). The serotonin transporter (SERT) transiently expressed in TC axons approximately from embryonic (E) day 15 to postnatal (P) day 10 reuptakes 5-HT at the TC synapse (Lebrand et al. 1998; Gaspar et al. 2003). Blockage of SERT, either genetically or pharmacologically, results in impaired topological TC innervation and organization of the barrel field in cortical LIV (Gaspar et al. 2003; Lee 2009; Miceli et al. 2013; Chen et al. 2015) as well as reduced expression of GABAergic markers important for inhibitory synapse formation (Guidotti et al. 2012). Hence, regulating extracellular 5-HT levels during the first 2 postnatal weeks is critical for proper TC synaptic transmission and consequently, maturation of the intracortical circuits (Chen et al. 2015).

Synaptic inhibition is crucial for proper sensory signal processing (Miller 2003; Wilent and Contreras 2005; Isaacson and Scanziani 2011) as microcircuits such as those which mediate feedforward inhibition (FFI) in cortical LIV allow the gating of incoming peripheral stimuli and preserve their spatio-temporal aspects (Gabernet et al. 2005; Roux and Buzsáki 2015). In S1 cortical networks, this is possible through the topologically organized projections of TC axons of the ventroposteromedial thalamic nucleus (VPM) onto both excitatory neurons, that is, spiny stellate and pyramidal cells, and inhibitory interneurons (in particular GABAergic parvalbumin positive fast spiking [FS] neurons) in the cortical LIV barrels (Porter et al. 2001; Devlin et al. 2005; Sun et al. 2006; Cruikshank et al. 2007, 2010; Daw et al. 2007; Hull and Scanziani 2007; Kimura et al. 2010). Since the thalamocortical afferents (TCAs) of the VPM project monosynaptically onto excitatory neurons, whereas the inhibitory input requires disynaptic transmission, this circuit allows a short time window (1–2 ms) for temporally relevant information to be integrated before the inhibitory input shunts any latent response (Miller et al. 2001; Swadlow 2003; Bruno and Sakmann 2006). Furthermore, FFI prevents excessive recurrent excitation of the extensively interconnected excitatory LIV neurons (Feldmeyer et al. 1999; Schubert et al. 2003). SERT dysfunction and consequently high extracellular 5-HT levels affect the topological organization of the barrel field as well as the expression of GABAergic markers (Cases et al. 1996; Persico et al. 2001; Salichon et al. 2001; Rebsam et al. 2002; Guidotti et al. 2012; Miceli et al. 2013; Chen et al. 2015), suggesting that it could affect the formation and maturation of the inhibitory circuits involved in mediating sensory integration within the input LIV of the barrel cortex. Here, we investigated the association between high extracellular 5-HT levels during development due to SERT knockout (Homberg et al. 2007) and the functioning of FFI circuits in controlling excitatory networks in LIV barrels of S1 using juvenile *Sert*$^{-/-}$ rats. Using electrophysiological, anatomical, molecular, and behavioral approaches, we found that reduced perisomatic inhibitory synaptic innervation of excitatory LIV neurons, reduced inhibitory drive due to a depolarized $GABA_A$ reversal potential (E_{GABA}), as well as a reduced membrane expression of the KCC2 chloride transporter; *Sert*$^{-/-}$ rats showed an increased excitability of LIV to LII/III pathways and integrated sensory information faster, making perceptually-based decisions with significantly fewer whisker contacts during a whisker-input-based spatial object localization task. These results show that the serotonergic homeostasis during brain development has a significant impact on the formation (see also Miceli et al. 2013) as well as on the functioning of sensory cortical networks and thus, consequently, on sensory perception.

Materials and Methods

Animals

Experiments were performed on male juvenile (postnatal (P) day 20–23, except the behavioral experiments which were performed between P21 and P28) Wistar rats. *Sert*$^{-/-}$(Slc6a4^{1Hubr}) rats were generated by ENU-induced mutagenesis (Smits et al. 2006). All animals were bred and reared in the Central Animal Laboratory of the Radboud University Nijmegen (Nijmegen, the Netherlands). Breeding animals were derived from outcrossing heterozygous (*Sert*$^{+/-}$) knockout rats for 8 generations. Experimental animals were derived from homozygous breeding. We genotyped the animals routinely in order to confirm their genetic background. Animals were supplied with food and water ad libitum and were kept on a 12:12 h light:dark cycle (lights on at 06:00 h). The light:dark cycle was inversed for the Gap Crossing behavioral experiment. All experiments were approved by the Committee for Animal Experiments of the Radboud University Nijmegen Medical Centre, Nijmegen, the Netherlands, and all efforts were made to minimize animal suffering and to reduce the number of animals used.

Electrophysiological Recordings

Slice Preparation

Acute TC slices from the rat somatosensory cortex containing the pathway from the thalamus to the barrel cortex (Agmon and Connors 1991) were used. Following anesthesia and decapitation, brain tissue containing the barrel cortex was excised, quickly removed from the skull, and stored in ice-cold artificial cerebrospinal fluid (ACSF) oxygenated with carbogen (95% O2, 5% CO2). ACSF consisted of (in mM): 124 NaCl, 1.25 NaH_2PO_4, 26 $NaHCO_3$, 1 $CaCl_2$, 5 $MgCl_2$, 3 KCl, 10 glucose at pH 7.4. The hemispheres were separated and cut with a 55° angle from the midline according to the rat brain coordinates of Land and Kandler (2002). The tissue block containing the region of interest was glued to a chilled Vibratome platform (Microm HM 650 V, Microm) and slices (300 μm thickness) were cut. The slices were stored in an incubation chamber containing carbogenated ACSF at room temperature for at least 1 h, then transferred to the recording chamber and submerged in 32 °C ACSF 124 NaCl, 1.25 NaH_2PO_4, 26 $NaHCO_3$, 2 $CaCl_2$, 1.8 $MgCl_2$, 3 KCl, 10 glucose at pH 7.4. at a flow rate of 1 mL/min.

Voltage-Clamp Recordings

LIV excitatory neurons were identified based on their perisomatic morphology using an upright microscope (Olympus) fitted with 2.5× and 40× objectives. The barrel field was visualized at low magnification and the individual cells were selected within the barrels at high magnification using an infrared enhanced quarter-field illumination (DGC, Luigs & Neumann).

Somatic whole-cell recordings were performed at room temperature using borosilate glass pipettes with a tip resistance of 4–6 MΩ. Patch pipettes were filled with (in mM): 115 $CsMeSO_3$, 20 CsCl, 10 Hepes, 2.5 $MgCl_2$, 4 Na_2ATP, 0.4 NaGTP, 10 Na-Phosphocreatine, 0.6 EGTA). Cells were selected at a minimum depth of −60 μm to retain the maximum network and minimize cutting artifacts. $GABA_A$/AMPA ratio recording was performed as previously described (Chittajallu and Isaac 2010) in AP5 (100 μM) where input onto LIV excitatory cells was evoked by placing a bipolar stimulation electrode in the thalamic afferents and applying a 200 μs pulse. The stimulation intensity was calibrated in order that the GABA (0 mV) response could be recorded in a range smaller than 1000 pA, where the same stimulation could induce a visible AMPA response at −70 mV which was usually in the range of 50 pA. The ratio of the peak $GABA_A$ mediated inhibitory postsynaptic currents (IPSC) amplitude (recorded at V_h 0 mV) to the peak amplitude of the AMPA receptor-mediated excitatory postsynaptic currents (EPSC) (recorded at V_h −70 mV), refers to the $GABA_A$/AMPA ratio. Thalamic release probability onto excitatory and FS interneurons was recorded as paired-pulse ratio (PPR) of evoked EPSCs at V_h −70 mV, at varying interstimulus intervals (ISIs; 50 and 100 ms) with a stimulation strength which could evoke an initial EPSC at −70 mV within a range of 50–200 pA. The latter was recorded using a K-gluconate based intracellular solution which allowed us to identify and characterize the firing response of FS interneurons as well as their intrinsic properties (see current-clamp recordings). For evoked IPSCs, a bipolar stimulation electrode was placed within the recorded LIV barrel at a minimum distance of 50 μm from the recorded cell, which was held at +10 mV. Paired-pulse stimulation was delivered as voltage or current pulses with a 200 μs pulse at different ISIs (50, 100, 200, and 500 ms). PPR was calculated as the ratio of Amplitude 2/Amplitude1. Miniature IPSCs (mIPSCs) were recorded at holding potential (V_h) of +10 mV in ACSF containing 1 μM TTX and 100 μM AP5 (Tocris Bioscience). Miniature excitatory postsynaptic currents (mEPSCs) were recorded at V_h −70 mV in ACSF containing 1 μM TTX and 100 μM PTX (Tocris Bioscience).

Current-Clamp Recordings

Somatic, whole-cell current clamp recordings, were performed using a K-gluconate based intracellular solution (13 KCl, 117 K-gluconate, 10 K-HEPES, 2 Na_2ATP, 0.5 NaGTP, 1 $CaCl_2$, 2 $MgCl_2$, 11 EGTA). FS interneurons were characterized for their resting membrane potential and passive and active intrinsic membrane properties by injection of a series of depolarizing pulses until reaching action potential firing. Electrophysiological data were not corrected for a liquid junction potential of approximately −10 mV. Inhibitory reversal potential was measured as previously described (Staiger et al. 2004). A bipolar stimulation electrode was placed within the thalamic afferents and a 200 μs pulse was applied until a first inhibitory postsynaptic potential (IPSP) could be observed in the recorded LIV neuron. After identification of the first IPSP, the stimulation strength was doubled to ensure a strong disynaptic inhibition and the recorded neuron was held at different membrane potentials using a voltage-clamp controlled current-clamp mode (from −80 to −40 mV). The time at which the peak IPSP (around V_h −40 mV) was observed was used to determine the membrane potential with zero net flow equal to 0 mV.

Signal Acquisition and Analysis

The signals were amplified (SEC-05LX; npi-electronics), filtered at 3 kHz, and digitized using a Power1401 interface (CED). Data were recorded, stored, and analyzed with PC-based software (Signal, CED). After recording, the slices were photographed in the bath chamber to document the topography of barrel-related columns and laminae as well as the respective position of the patch electrode.

Histochemistry and Neuronal Quantification

Tissue Processing and Immunofluorescence

Histology was performed on TC slices following intracardial perfusion (4% paraformaldehyde in phosphate-buffered solution (PBS) 0.1 M, pH 7.4). The hemispheres were separated and cut with a 55° angle from the midline according to the rat brain coordinates of Land and Kandler (2002) to preserve pathway from the thalamus to S1 and 60 μm slices were embedded (2% agarose) and cut using a vibratome (Microm HM 650 V, Thermo Fisher Scientific). Slices were rinsed and blocked overnight at 4 °C in 10% normal goat serum (Invitrogen) and 10% normal donkey serum (D9663, Sigma-Aldrich) in PBS containing 0.05% Triton-X and 1% BSA on a shaking Table at 4 °C. Primary antibodies chicken-anti NeuN (1:500; ABN91, Millipore), mouse-anti GAD67 (1:1000; MAb5406, Millipore), and rabbit-anti GABA (1:500; A2052, Sigma-Aldrich) were incubated for 48 h 4 °C to ensure thorough tissue penetration. Secondary antibodies, Alexa Fluor 488-AffiniPure donkey anti-chicken (1:200; 703-545-155, Jackson Immunoresearch), Alexa Fluor 568 goat anti-mouse (1:200; Invitrogen) and Alexa Fluor 647 goat anti-rabbit IgG (1:200; Invitrogen) were incubated at room t° for 3 h. Slices were mounted in Dako fluorescent mounting medium (Dako North America Inc.). Negative control experiments were performed by incubation without primary antibodies.

Image Acquisition

Mosaic scans with a voxel size of 1.52 × 1.52 × 0.99 μm were taken using the Leica TCS SP5 confocal microscope equipped with Argon-, DPSS 561-, and HeNe 633-lasers at a magnification of ×20. Throughout imaging, the same laser power and photomultiplier settings were used. Large multi-tile images were created using the automated stitching plugin provided in the Leica Application Suite Advanced Fluorescence software. Using the GAD67 channel, the same S1 column was manually selected in 6 subsequent sections for each animal. The selected columns were then analyzed using a Matlab-based automated cell counting method that uses a combination of filtering and correction methods to collect data on the amount of inhibitory and excitatory neurons within a barrel column (see below).

Automated Cell Counting Analysis

All image analyses were performed using custom-written Matlab routines running on Matlab 2012b with Image Processing Toolbox (Mathworks). For localization of the positively stained nuclei, we first applied a 3D median filter (Region of interest: 3 × 3 × 3 pixels) and the resulting image was used for vignette correction (Zheng et al. 2009). This process ensured homogenous illumination throughout the cortical volume and accounted for the intensity variation in the signal. For background subtraction, the background was estimated by dilation (disk, 15 pixels in radius). To increase the SNR and amplify the signal from weakly stained neurons, we applied contrast-limited adaptive histogram equalization (8 × 8 tiles). Images were then converted to the grayscale (256 levels) before the separation of foreground (i.e., signal) from the background using an adaptive threshold (2-level; Otsu 1979). Nuclear localization was performed using a modified

watershed (Meyer 1994), so-called the marker-based watershed method; Markers were calculated by applying regional maxima transform on (grayscale) foreground pixels smoothed by morphological opening-by-reconstruction operation (Vincent 1993). To ensure accurate detection of cell boundaries image dilation (1 pixel) is applied to the B&W foreground before watershed segmentation. Finally, objects with a surface volume <70 pixels (empirically determined) are removed by morphological opening. Cell density is calculated from tissue volume measured by confocal microscopy. The collected data were binned into 20 bins per section, which were combined to represent their respective layers. Neuronal densities and IN-to-neuron ratios were analyzed for the entire column and per layer.

Statistical Analysis of the Reliability of Automated Counting

Three human observers independently counted varying number of 3-D image stacks from different antibody staining, using Vaa3D software (Peng et al. 2010). Three identical copies of each image stack were placed in the manual counting data-set in random order, and the human observers did not notice the repeated appearing of the same samples.

Quantification of Inhibitory Boutons onto Somata of Excitatory LIV Neurons

Immunofluorescence, Image Acquisition, and Analysis

Tissue was acquired and processed as previously described for the neuronal quantification immunohistochemistry protocol in the exception that a lower Triton-X concentration (0.01%) was used to prevent disruption of membrane proteins. Using a Zeiss Axio Imager Z1 fluorescent microscope, equipped with an ApoTome system, the center of a LIV barrel was localized at 20× based on dense GAD67 immunofluorescence labeling. Increased ×63 magnification was then used to image and select single excitatory neuronal cell bodies within a barrel, based on a NeuN positive and GABA-negative immunolabeling. A total of 91 $Sert^{+/+}$ and 82 $Sert^{-/-}$ LIV neurons were photographed and quantified using NIH ImageJ software. Perisomatic inhibitory varicosities were defined as small (0.5–1 μm) GAD67-positive puncta located within 1 μm of a NeuN positive and GABA-negative cell body. Circumference of neurons was calculated and perisomatic inhibitory GAD67 puncta were normalized to circumference in μm. Data are given as GAD67 puncta/μm.

Determination of KCC2 and NKCC1 Protein Concentration

Tissue Acquisition and Cross-Linking

Acute thalamocortical slices from P21 $Sert^{+/+}$ ($n = 12$) and $Sert^{-/-}$ ($n = 12$) were obtained in the same manner as for electrophysiological recordings (see above). Punches of barrel cortex from 3 subsequent 300 μm slices submerged in ice-cold ACSF were taken bilaterally using a 2 mm micropunch (Harris Inc.), following stereotactic coordinates of Land and Kandler (2002), snap frozen in liquid nitrogen and stored at 80 °C. Cell surface protein fractions were extracted using the BS^3 crosslinking method (Kasri et al. 2009) using 1 mM of the chemical crosslinking agent (BS^3, #21580, Thermo Fisher Scientific) in ice cold PBS. The crosslinking reaction was quenched by adding ice-cold 50 mM Tris-HCl (pH 8.0). Samples were homogenized in ice-cold RIPA buffer (150 mM NaCl, 1% Triton X-100, 0.5% Na-deoxychelate, 0.1% SDS, 50 mM Tris pH 8.0) containing protease inhibitors (Roche Holding AG) and phosphatase inhibitors (Roche Holding AG). Tissue homogenization was achieved by 10 rotations of a pestle in the Eppendorf tube. Subsequently, the samples were placed in a rotator at 4 °C for 30 min followed by centrifugation at 13 000 rpm at 4 °C for 20 min. The supernatant was transferred to a new tube and the pellet was discarded. A fraction of the supernatant was taken for determination of the protein concentration using the bicinchoninic acid (BCA)-assay (Thermo Fisher Scientific). Throughout these procedures, pairs of $Sert^{+/+}$ and $Sert^{-/-}$ samples were processed in parallel to minimize variability. Protein concentration was determined, samples were diluted to equal concentrations and incubated with 50 mM Dithiothreitol in Laemmli Sample Buffer (Bio-Rad Laboratories, Inc.) at 95 °C for 5 min.

Western Blotting and Analysis

Samples were resolved in 4–15% polyacrylamide gels (Bio-Rad Laboratories, Inc.). Proteins were transferred to a nitrocellulose membrane (Bio-Rad Laboratories, Inc.). Membranes were blocked for an hour in 5% nonfat dry milk in PBS-Tween (0.05%) and incubated in the following primary antibodies (diluted in PBS-Tween 0.05% containing 1% nonfat dry milk): polyclonal rabbit-anti KCC2 (1:1000; ab49917, Abcam), polyclonal rabbit-anti NKCC1 (1:500; ab59791, Abcam), or monoclonal mouse anti-γ-tubulin (1:2000; T5326, Sigma-Aldrich) overnight at 4 °C. After an hour of extensive washing in PBS-Tween (0.05%), membranes were incubated in horseradish peroxidase conjugated antibodies (1:8000) in PBS-Tween (0.05%) containing 1% nonfat dry milk; goat anti-rabbit IgG (#G21234, Invitrogen) for KCC2 and NKCC1 and goat anti-mouse IgG (#115-035-062, Jackson ImmunoResearch) for γ-tubulin. After incubating for 1 h at room temperature, blots were washed extensively again and revealed using the SuperSignal West Femto or Pico Chemiluminescent Substrate (Bio-Rad Laboratories, Inc.).

Western blots were analyzed using the Bio-Rad Image Lab 5.0 software. Due to crosslinking, high molecular weight multimeric complexes were formed that remained in the top portion of the polyacrylamide gels forming multiple bands, which was analyzed in its entirety. A measure for surface expression of KCC2 and NKCC1 was obtained by dividing the intensities of the crosslinked (surface) fraction by the monomeric (internal) fraction (Blaesse et al. 2006).

Multi Electrode Array recordings

For investigating stimulus-evoked intracortical signal propagation, we used extracellular recordings of local field potentials (LFPs) in slices mounted on multi electrode arrays (MEAs) kept under submerged conditions (identical to the conditions described above for whole cell patch clamp recordings and following a protocol described previously, Bakker et al. 2009). In brief, we used uncoated standard MEA chips (Multichannel Systems) containing 60 TiN electrode with a diameter of 30 μM spaced 200 μM center to center. The slices were positioned in such a way that the fourth row of MEA electrodes was aligned to cortical LIV and kept in place by a harp grid. This way all cortical layers were covered by at least one row of electrodes while vertically each barrel associated column was covered by 1–2 columns of MEA electrodes (see Fig. 6A). We allowed 30 min of incubation for the tissue to settle and ensure good connection with the MEA electrodes. Pictures were taken for later assignment of electrodes to cortical columns and layers during analysis.

We applied electrical stimulation as monophasic voltage pulses (200 μs at −1000 mV) by a MEA electrode that was aligned with a LIV barrel of interest (see Fig. 6A) using a stimulus

generator (STG2004, Multichannel Systems). Recording electrodes were blanked from 20 µs before until 100 µs after the pulse. Signals from the MEA electrodes were band pass filtered (0.1 Hz high pass filter and 3 kHz low pass filter), acquired by the PC-based data software MC Rack (Multichannel Systems) and digitized at a sampling rate of 10 kHz. Each stimulation protocol was repeated 8 times at 10 s intervals.

Pharmacology

We pharmacologically dissected the main components of stimulus-evoked LFPs. After the standard 30 min incubation in ACSF and recording of the stimulus-evoked LFPs, we added in a first step CNQX (5 µM, Sigma-Aldrich) in order to block AMPA receptor-mediated responses and in a second step, following another 30 min incubation, we added TTX (1 µM, Sigma-Aldrich) in order to also block voltage-gated sodium channels and thus action potential generation in the slice. Stimulus-evoked LFPs were recorded during each of the 3 conditions. LFPs typically consisted of a more or less prominent TTX sensitive fast action potential volley (within 2 ms post stimulus, see Bakker et al. 2009), followed by a slower negative, mainly CNQX sensitive AMPA component (see also Fig. 6*B*) representing local postsynaptic excitatory activity.

Analysis and Creation of Average Maps of Intracortical Excitatory Signal Propagation

MEA analysis was carried out with a custom made Matlab-based analysis toolbox (MEAMEA, developed in house). Based on the averages over 8 recorded sweeps, for each electrode we determined the negative peak amplitude of the synaptic excitatory component. Pictures were analyzed for the position of columns and layers and used to determine the layer and column-specific LFP responses. LFPs recorded from electrodes within the cortical column containing the stimulated LIV barrel were assigned to home column (HC) responses, those within the adjacent cortical column to neighboring column (NC) responses. For the quantitative analyses for each layer of interest in HC and NC, the electrode delivering the strongest LFP responses was considered. For the construction of genotype-specific average maps of excitatory signal propagation, including a visualization of confidence levels of evoked responses, we used a method to project individual response maps into a template map (Staiger et al. 2015). In brief, we matched the slice-specific laminar and columnar cytoarchitecture with a template using vertical and horizontal scaling. This procedure involved, as a first step, translating, scaling, and rotating LFP response maps with known layer and column-specific positioning of the electrodes until an optimal match with a template's center barrel position, overall barrel size, slice orientation, and pial surface was obtained. We estimated individual confidence levels that the averaged activity $\bar{x}$ at a given point differed from zero with $\zeta = 2 \cdot T\left(\frac{\bar{x} \cdot \sqrt{n}}{\sigma}, n\right) - 1$, where n was the number of contributing slices, σ the sample standard deviation, and T the cumulative Student's t-distribution. For display purposes, only those template grid points to which at least 3 slices contributed ($n \geq 3$) and for which $\zeta \geq 68.3\%$ (zero activity excluded by "one sigma") were considered further.

Gap-Crossing Paradigm

Tactile object localization training was performed on the gap-crossing task under no-visible light (Celikel and Sakmann 2007). Animals did not receive any reward for successful task execution, nor did they receive any whisker deprivation. The training was performed on the automated version of the paradigm (Voigts et al. 2008, 2015) where the target position was controlled by linear actuators. The position of the target platform was drawn from a Gaussian distribution and the target position was set prior to the onset of the trial. The mean of the distribution was increased (range: 3–7) and the variance was reduced (range: 1–3) with increased number of sessions to ensure that animals can be tested in large range of tactile distances. This training procedure also compensated the body growth across days.

The training lasted 5 days starting from postnatal day (P) 23. Two sessions of habituation to the apparatus on P21 and P22 were performed before animals were exposed to a gap. The entire first session and the first half of second habituation session were performed under white light. Each training session lasted for 30 min or 20 successful trials (whichever came first). A high-speed camera (PIKE AVT F-032B) positioned above the target platform in conjunction with infrared backlights (wavelength = 820 nm; NERLITE) placed under the elevated platforms was used to visualize whisker-based tactile exploration of the target as described before (Voigts et al. 2015).

Automated Analysis of Tactile Exploration Statistics

All image analyses were performed using custom-written Python routines using the OpenCV, Numpy, Scipy, and StatsModels toolboxes. A background image was computed as the average of 30 frames taken before the animal entered the field of view and subtracted from all the frames. Platform edges were detected in this background picture as the positions of a transition from a low to a high brightness in the illumination. The nose was assumed to be the dark point closest to the target platform edge as detected after automated adaptive thresholding (Otsu 1979). Crossing time was defined as the moment the animal's nose has passed the platform edge by more than 20 pixels. The contacts were determined as follow: A one-pixel-high line was extracted on each side of the target platform edge for every frame. From these lines 2 spatio-temporal images were constructed where the horizontal axis is the position along the platform edge and the vertical axis is time. In this representation, whiskers are V-shaped objects: During the protraction phase the whisker is coming closer to the center and during the retraction phase it is going back to the sides. After application of a median filter, those V-shaped objects were detected and labeled through a connected-components analysis. Whiskers detected on one side of the platform were assigned to the ones detected on the other side based on geometric proximity. If a whisker was detected before but not after the platform edge then it was considered to be a contact. This approach, without requiring us to trace the entire whisker length, yielded the number of contacts occurring on each frame. Human observers independently analyzed a random subset of the trials to confirm the accuracy of the automated count. Compared with the previous algorithms for whisker tracking in freely moving animals (Voigts et al. 2008) this approach provided rapid analysis of tactile exploration without any whisker deprivation. The time series were further analyzed by genotypes and gap distances. All statistical tests are 2-sided independent sample t-tests. Values are reported as mean ± standard error of the mean, in the text as well as on graphs with a shaded area.

Results

Reduced Efficiency of FFI at the LIV Thalamocortical Synapse of *Sert*$^{-/-}$ Rats

Efficient integration of sensory input within the circuitry of the primary somatosensory cortex requires coincidence detection

of temporally correlated synaptic activity through feedforward mechanisms, which require proper excitatory/inhibitory function (Higley and Contreras 2003; Celikel et al. 2004; Foeller et al. 2005; Marik et al. 2010). In order to test the efficiency of FFI, we first verified that LIV excitatory neurons of both *Sert*$^{-/-}$ and *Sert*$^{+/+}$ rats received excitatory and inhibitory input following thalamic fiber stimulation. We measured excitatory postsynaptic potentials (EPSPs) and IPSPs onto LIV excitatory neurons using whole-cell current clamp (CC) recordings in combination with orthodromic stimulation of TCAs via a bipolar stimulation electrode positioned in the white matter below LVI (Staiger et al. 2004, Fig. 1A). We identified excitatory LIV *Sert*$^{+/+}$ and *Sert*$^{-/-}$ neurons based on their somatic appearance and their action potential firing pattern and classified them as regular spiking or burst spiking as previously described (Miceli et al. 2013, Supplementary Fig. 1). All excitatory neurons had a stable resting membrane potential of <−60 mV. For morphological confirmation, a subset of LIV excitatory cells ($n = 20$) were filled with biocytin and classified as being either spiny stellate (SpSt; $n = 11$) or pyramidal (Pyr; $n = 9$) neurons (Supplementary Fig. 1). In agreement with our previous study (Miceli et al. 2013), we found no genotypic differences in the basic intrinsic electrophysiological properties of either excitatory cell classes (Miceli et al. 2013, Table 1). In all recorded excitatory LIV cells of both *Sert*$^{+/+}$ and *Sert*$^{-/-}$ rats, TCA stimulation reliably induced a monosynaptic EPSP in CC at a holding potential (V_h) of −65 mV, without any genotype-specific difference in the stimulation strength that was needed to induce an EPSP of 2.5 mV (Fig. 1A, B). Increasing the stimulation intensity resulted in higher amplitude EPSPs until the feedforward inhibitory circuits were recruited, which induced a fast disynaptic hyperpolarizing IPSP in all recorded neurons of both genotypes. In contrast to the direct excitatory TC inputs onto the LIV cells, on average, the induction of the disynaptic IPSP required stronger TCA stimulation in *Sert*$^{-/-}$ than in *Sert*$^{+/+}$ rats (Fig. 1A,B, *Sert*$^{+/+}$: $n = 10$, *Sert*$^{-/-}$: $n = 13$, $P < 0.05$). One should note, however, that due its technical limitations in calibration, electrical TCA stimulation only allows a coarse comparison of TC innervation strength between the 2 genotypes. Due to the lack of cell-type specific differences in stimulus-evoked responses upon TCA stimulation we considered LIV excitatory neurons as one group.

We investigated thalamic integration of excitatory/inhibitory inputs by measuring GABA ($V_h = 0$ mV) and AMPA ($V_h = -70$ mV) currents onto LIV excitatory neurons of both genotypes following strong thalamic afferent stimulation in whole-cell voltage clamp. GABA/AMPA ratios were 43% lower in *Sert*$^{-/-}$ rats (Fig. 1B; *Sert*$^{+/+}$ 4.27 ± 0.90, $n = 13$; *Sert*$^{-/-}$ 2.45 ± 0.34, $n = 17$; $P < 0.05$) demonstrating a reduced inhibitory control of the excitatory LIV neurons.

As a next step, we tested whether in *Sert*$^{-/-}$ rats, the FFI was affected by an altered intrinsic neuronal excitability and/or changes in the synaptic release probability for TC input onto 2 relevant cortical target cell populations, that is, excitatory as well as FS inhibitory neurons, in LIV. To this end, we recorded LIV FS inhibitory neurons (*Sert*$^{+/+}$ $n = 6$, *Sert*$^{-/-}$ $n = 6$), which were identified based on their ovoid soma shape as well as their high frequency, non-adapting AP firing pattern (Supplementary Fig. 2A; Porter et al. 2001). The intrinsic membrane properties of inhibitory LIV FS neurons were similar across both genotypes (Table 1), implying no change in the intrinsic excitability. Recordings of TCA induced EPSCs in inhibitory FS LIV neurons showed that those of *Sert*$^{-/-}$ rats require stronger TCA stimulation than those *Sert*$^{+/+}$ in order to reach an excitatory input current of a certain magnitude (Supplementary Fig. 2B,C; *Sert*$^{+/+}$ $n = 6$, *Sert*$^{-/-}$ $n = 6$; $P < 0.05$). We furthermore tested the release probability of the TC synapses using paired-pulse stimulation of the TCAs (Stevens 2003). Using whole-cell voltage clamp (V_h −70 mV), stimulation of TCAs at ISI of 50 and 100 ms revealed no significant changes in the PPR of excitatory current responses onto excitatory LIV neurons (Supplementary Fig. 1D; 50 ms: *Sert*$^{+/+}$ 0.97 ± 0.06, $n = 18$; *Sert*$^{-/-}$ 1.03 ± 0.11, $n = 17$; $t(28) = 0.47$, $P = 0.65$; 100 ms: *Sert*$^{+/+}$ 1.06 ± 0.08; *Sert*$^{-/-}$ 1.00 ± 0.08, $t(33) = 0.48$, $P = 0.63$) as well as onto inhibitory FS cells

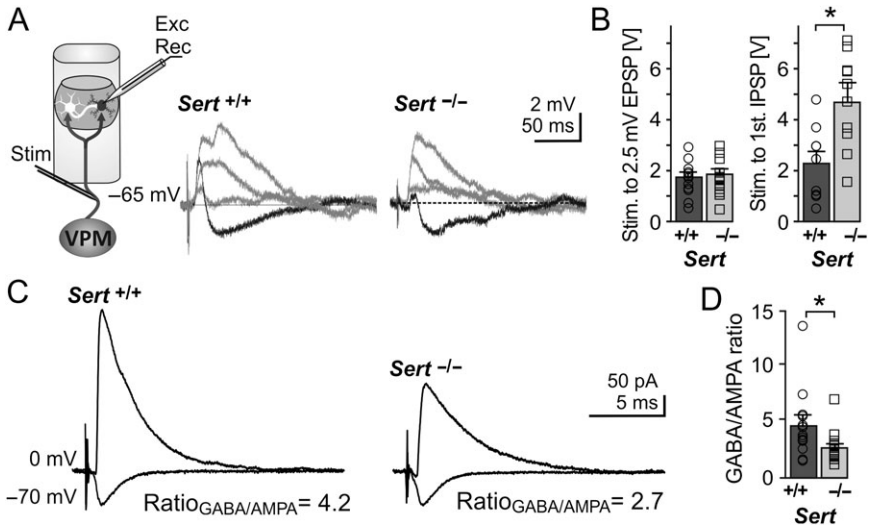

Figure 1. *Sert*$^{-/-}$ rats show reduced FFI onto LIV excitatory neurons (*A*) Left, schematic of the recording depicting bipolar stimulation in the TCAs originating from the VPM with whole cell recording of a monosynaptic excitatory input and disynaptic inhibitory input onto an excitatory neuron within a LIV barrel. Middle, example current clamp recording showing input onto a LIV excitatory neuron following TCA stimulation with increasing stimulation strength (response to strongest stimulation resulting is given in black). Strongest stimulation resulted in truncation of the EPSP by disynaptic IPSP in both *Sert*$^{+/+}$ and *Sert*$^{-/-}$. (*B*) Histograms showing the TCA stimulation strength (as voltage pulses) needed to evoke an EPSP of 2.5 mV (left, *Sert*$^{+/+}$: $n = 1$, *Sert*$^{-/-}$: $n = 14$) and strength needed to induce the first IPSP (right, *Sert*$^{+/+}$: $n = 10$, *Sert*$^{-/-}$: $n = 13$) LIV excitatory neurons. (*C*) Representative voltage clamp recordings depicting approximate mean of *Sert*$^{+/+}$ and *Sert*$^{-/-}$ GABA currents at V_h = 0 mV and AMPA currents at V_h = −70 mV. (*D*) Histogram of mean GABA/AMPA ratio of *Sert*$^{+/+}$ ($n = 13$) and *Sert*$^{-/-}$ ($n = 17$) rats recorded in voltage clamp. Data are represented as mean ± SEM, *$P < 0.05$ (*t*-test).

(Supplementary Fig. 2B,C). Furthermore, we tested the reversal potential of the fast disynaptic $GABA_A$ mediated inhibitory input (E_{GABA}) onto LIV excitatory cells using a strong TCA stimulation. While recording excitatory LIV neurons in current clamp at varying membrane potentials (between −80 and −40 mV) we observed a significantly depolarized inhibitory reversal potential in $Sert^{-/-}$ LIV excitatory neurons (Fig. 2; $Sert^{+/+}$ −68.18 ± 1.67 mV, n = 18; $Sert^{-/-}$ −62.47 ± 2.00 mV, n = 19; $t(35) = 2.20$; $P < 0.05$).

Taken together, these results show that the FFI circuits of $Sert^{-/-}$ rats possess a reduced efficiency in mediating inhibitory control of excitatory LIV neurons. Beyond finding an indication for a weaker excitatory TC drive of the presynaptic FS inhibitory neurons, the reduced efficiency in mediating inhibitory control of excitatory LIV neurons was supported by a 43% reduction in GABA/AMPA ratio as well as a depolarizing shift in E_{GABA}. Next, we investigated the intracortical network mechanisms that could contribute to this reduction in inhibitory drive within LIV.

Reduced Inhibitory Synapses onto Somata of LIV Excitatory Neurons of $Sert^{-/-}$ Rats

SERT dysfunction has previously been shown to alter the migration of inhibitory neurons during embryonic development (Riccio et al. 2009; Frazer et al. 2015) and result in altered cellular laminarization in various cortical areas (Altamura et al.

Table 1 Electrophysiological properties of LIV excitatory and FS interneurons

	Regular spiking		Intrinsically bursting		Fast spiking	
Properties	$Sert^{+/+}$ $n = 21$	$Sert^{-/-}$ $n = 27$	$Sert^{+/+}$ $n = 19$	$Sert^{-/-}$ $n = 18$	$Sert^{+/+}$ $n = 6$	$Sert^{-/-}$ $n = 6$
Passive intrinsic						
V_{rmp} [mV]	−69.5 ± 1.5	−67.8 ± 1.4	−70.1 ± 1.0	−71.6 ± 3.5	−79.8 ± 1.3	−75.4 ± 3.0
R_m [MΩ]	156.6 ± 13.0	131.1 ± 13.2	149.2 ± 14.0	140.9 ± 15.2	182.3 ± 41.8	182.2 ± 48.5
τ_m [ms]	20.5 ± 1.9	18.9 ± 1.8	17.2 ± 1.8	17.5 ± 1.9	11.0 ± 1.3	11.5 ± 1.8
Active intrinsic						
AP threshold [mV][a]	−37.8 ± 1.1	−36.7 ± 1.1	−35.0 ± 1.1	−38.4 ± 2.0	−39.8 ± 1.0	−41.3 ± 1.2
AP amplitude [mV]	79.2 ± 1.6	73.6 ± 5.9	73.2 ± 3.2	77.4 ± 4.7	68.2 ± 3.6	59.5 ± 5.0
AP halfwidth [ms]	1.3 ± 0.1	1.5 ± 0.1	1.4 ± 0.1	1.3 ± 0.1	0.8 ± 0.1	0.8 ± 0.1
First ISI [ms][a]	45.7 ± 6.6	52.8 ± 7.4	10.5 ± 2.5	7.5 ± 2.5	20.8 ± 3.1	30.8 ± 4.0
Third ISI [ms][b]	44.8 ± 2.3	46.2 ± 3.1	39.7 ± 1.4	41.4 ± 2.5	23.4 ± 3.1	30.4 ± 3.6
Ninth ISI [ms][b]	62.1 ± 2.0	59.0 ± 1.6	66.5 ± 2.8	67.2 ± 4.4	23.3 ± 2.9	29.8 ± 3.1
Ninth/Third ISI ratio	1.2 ± 0.1	1. 5 ± 0.1	1.7 ± 0.1	2.3 ± 0.1	1.0 ± 0.1	1.0 ± 0.0
fAHP [mV]					13.8 ± 2.3	13.4 ± 2.1

[a]Active properties were measured by just suprathreshold stimulation, eliciting 2–4 APs.
[b]Active properties were measured by stronger depolarizing current injection, eliciting 10–14 APs. No significant differences were found between regular spiking, intrinsically bursting or FS interneurons across both genotypes.
Data are means ± SEM. ISI, interstimulus interval; fAHP, fast hyperpolarizing potential.

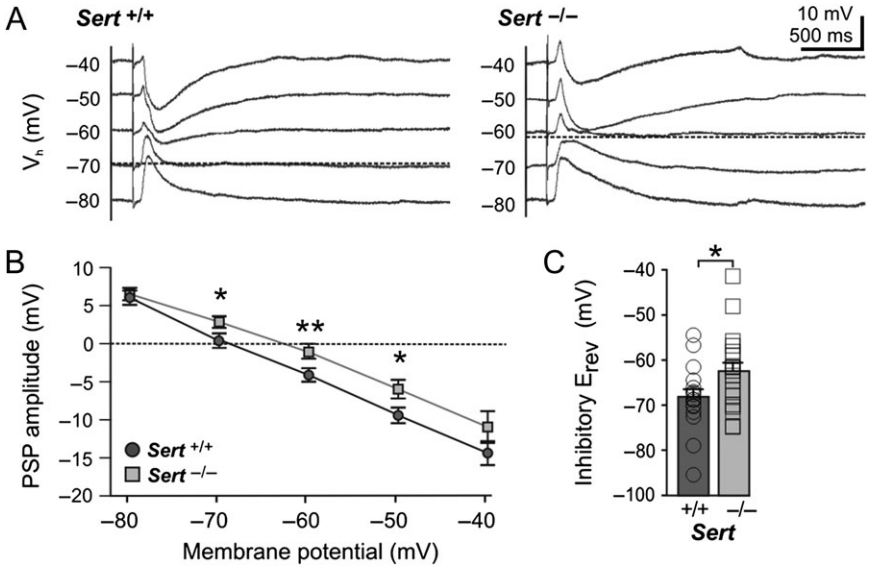

Figure 2. $Sert^{-/-}$ rats show a depolarized inhibitory reversal potential in LIV excitatory neurons. (A) Example current clamp traces of postsynaptic responses recorded in LIV excitatory neurons at different membrane potentials in (−80 to −40 mV) following maximal bipolar stimulation (2 × stimulation intensity for eliciting a first truncating IPSP) of TCAs of $Sert^{+/+}$ and $Sert^{-/-}$. (B) Plot of postsynaptic potential amplitudes at different holding potentials in $Sert^{+/+}$ (n = 18) and $Sert^{-/-}$ (n = 19). (C) Histogram of mean reversal potential in $Sert^{+/+}$ and $Sert^{-/-}$ rats, which was determined at x-intercept and averaged. Data are presented as mean ± SEM, *$P < 0.05$ (t-test).

2007). Therefore, a reduced GABA/AMPA ratio and subsequent reduction in inhibitory control in the FFI circuit of *Sert*$^{-/-}$ rats could be mediated by a lower number of inhibitory neurons along a cortical column. To evaluate the density and laminar distribution of excitatory and inhibitory neurons, we performed immunohistochemistry on TC slice preparations and reconstructed a barrel column at soma resolution to measure neuronal densities of excitatory and inhibitory neurons (Fig. 3A–C; see Materials and Methods). The total number of neurons per tissue volume was determined by counting NeuN positive (NeuN$^+$) somata and that of presumed inhibitory and presumed excitatory cells by counting GABA positive (GABA$^+$) and NeuN$^+$/GABA$^-$ somata, respectively. We used glutamate decarboxylase 67 (GAD67) labeling to determine the dimensions of the individual LIV barrels (Meyer et al. 2010). We found no significant genotypic differences between the total columnar densities of NeuN$^+$/GABA$^-$ somata (presumed excitatory neurons, *Sert*$^{+/+}$ 2.32 E+06 ± 4.84 E+04/mm^3, $n = 13$; *Sert*$^{-/-}$ 2.50 E+06 ± 3.67 E+04/mm^3, $n = 10$; $F(1,5) = 2.02$, $P = 0.08$) and GABA$^+$ somata (presumed inhibitory neurons, *Sert*$^{+/+}$ 3.92 E+05 ± 8.18 E+03/mm^3; *Sert*$^{-/-}$ 4.25 E+05 ± 1.62 E+04/mm^3, $F(1,5) = 1.70$, $P = 0.14$) as well as in the ratio of GABA$^+$ neurons to total NeuN$^+$ neurons (*Sert*$^{+/+}$ 22.37 ± 0.22%; *Sert*$^{-/-}$ 23.13 ± 0.23%, $F(1,5) = 2.17$, $P = 0.06$). Likewise, we found no significant genotypic differences in the layer specific numbers and densities across the cortical column (Fig. 3D–F). These findings argue that SERT loss of function does not alter the number, density or laminar location of GABA$^+$ neurons in the juvenile rat barrel cortex.

With unaltered neuronal densities within the barrel circuits, a lower GABA/AMPA ratio on the synaptic level could be indicative of either a reduced GABAergic input, an increased AMPAergic input or a combination of both. To directly quantify the number of GABAergic inputs any given LIV excitatory neuron receives, we first classified individual NeuN$^+$/GAD67$^-$ somata as presumed excitatory neurons within LIV barrels (Fig. 4A). Since GAD67 is expressed throughout GABAergic neurons and thus also in presynaptic terminals of inhibitory neurons (Pinal and Tobin 1998; Huang et al. 2007) we quantified GAD67 puncta that were localized onto the soma of excitatory cells, a typical innervation domain of inhibitory FS LIV basket cells (Huang et al. 2007), as a measure of perisomatic inhibitory synaptic contacts. We observed a 18% reduction in perisomatic bouton numbers in *Sert*$^{-/-}$ rats, indicating fewer inhibitory synapses targeting LIV excitatory neurons (Fig. 4B; *Sert*$^{+/+}$ 0.30 ± 0.01 synapses/µm, $n = 82$; *Sert*$^{-/-}$ 0.24 ± 0.01 synapses/µm, $n = 91$; $t(177) = 5.95$, $P < 0.001$). Additionally, we functionally assessed the strength and number of both excitatory and inhibitory synapses onto LIV excitatory neurons, using whole-cell voltage clamp recordings of miniature postsynaptic currents. We found no differences in mEPSC frequency (*Sert*$^{+/+}$ 5.87 ± 0.36 Hz, $n = 12$; *Sert*$^{-/-}$ 6.00 ± 0.48 Hz, $n = 16$; $t(21) = 0.20$, $P = 0.42$) or amplitude (Fig. 4C; *Sert*$^{+/+}$ 10.44 ± 0.48 pA; *Sert*$^{-/-}$ 10.70 ± 0.44 pA; $t(21) = 0.36$, $P = 0.36$), thereby excluding any change in AMPA receptor expression. However, in *Sert*$^{-/-}$ rats, mIPSCs were significantly reduced in both their frequency (*Sert*$^{+/+}$ 4.4 ± 0.3 Hz; *Sert*$^{-/-}$ 3.4 ± 0.3 Hz; $t(31) = 2.34$, $P < 0.01$) and amplitude (Fig. 4D; *Sert*$^{+/+}$ 33.5 ± 1.9 pA; *Sert*$^{-/-}$ 28.2 ± 1.9 pA; $t(31) = 1.95$, $P < 0.01$).

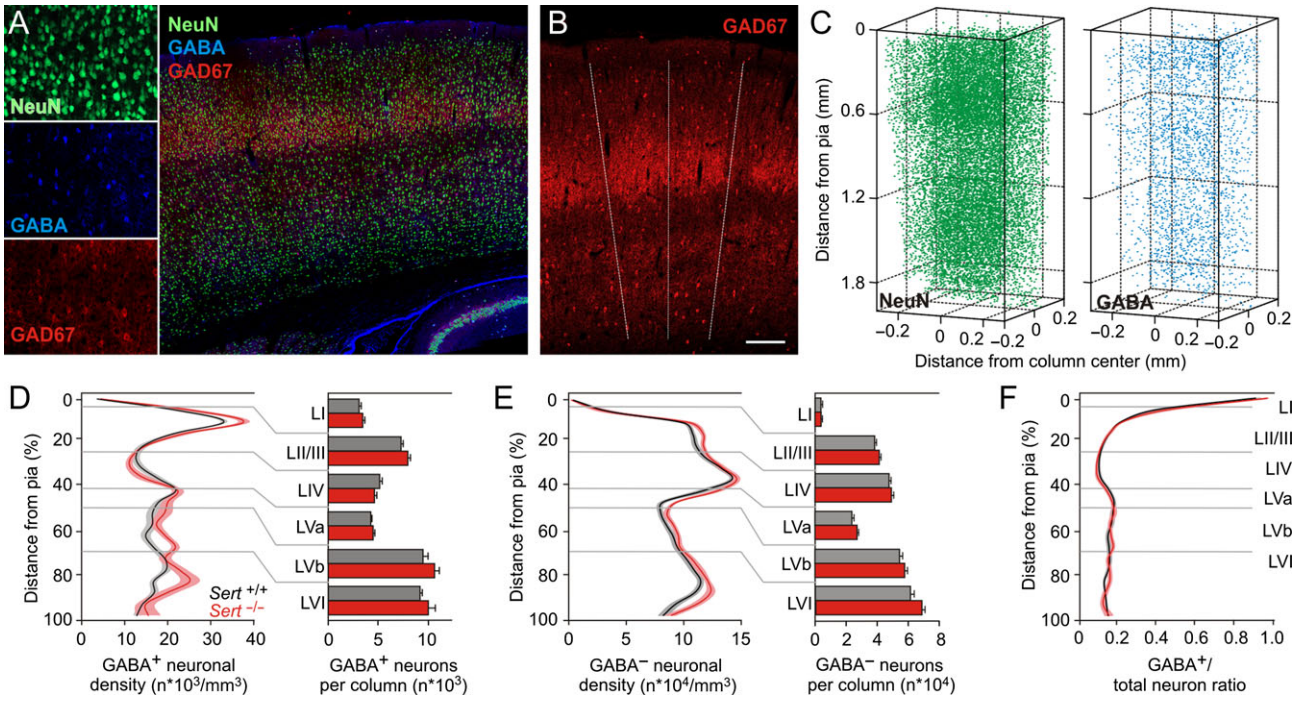

Figure 3. Reduction in inhibitory control in *Sert*$^{-/-}$ rat is not due to changes in density or laminar distribution of inhibitory neurons within a cortical column. (*A*) Left, photomicrographs of single fluorescence channels for all neuron identification (NeuN), interneuron identification (GABA), and barrel identification (GAD67). Right, photomicrograph showing merged immunolabeling of one TC slice (60 µm) with GAD67, NeuN and GABA positive neurons. (*B*) The limits of barrel borders were determined from the GAD67 labeling in LIV and extrapolated to all layers (dashed lines). (*C*) Excitatory and inhibitory neurons distribution were quantified from 6 subsequent slices (total 360 µm). Left, NeuN$^+$ neuron density distribution and right, GABA$^+$ neuron distribution were used to identify excitatory (NeuN$^+$, GABA$^-$ somata) and inhibitory (GABA$^+$ somata) neuron distribution across a barrel column. (*D*,*E*) Normalized (from Pia to white matter) distribution of excitatory and inhibitory neuronal densities along a cortical column and histogram of layer quantifications (*Sert*$^{+/+}$ 13 barrels in 5 animals; *Sert*$^{-/-}$ 10 barrels in 5 animals) shows no significant changes in the density and laminar distribution of neuronal populations in *Sert*$^{-/-}$ rats. (*F*) GABA$^+$ to total neuron ratio show absence of difference in *Sert*$^{-/-}$ rat. Two-way ANOVA with Bonferroni correction was used for data in *D*, *E*, and F. All data are presented as mean ± SEM.

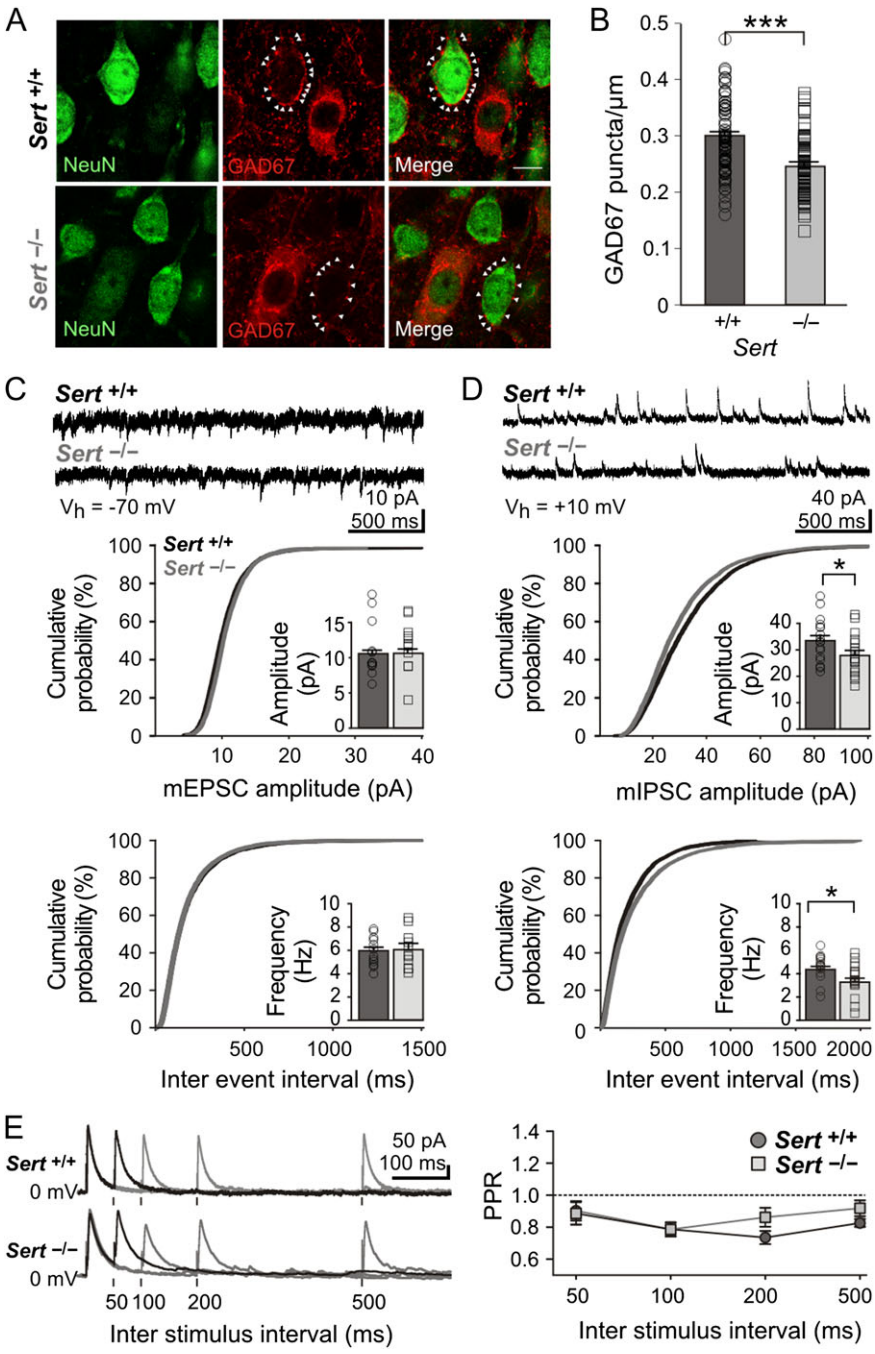

Figure 4. *Sert*$^{-/-}$ rats show a reduced number of perisomatic inhibitory boutons onto excitatory LIV neurons. (*A*) Fluorescent photomicrographs of LIV excitatory neurons (NeuN^{+}/Gad67^{-}) used for quantification of perisomatic GAD67 puncta/µm in *Sert*$^{+/+}$ and *Sert*$^{-/-}$ rats. White arrows mark puncta onto a representative soma of a pyramidal cell. (*B*) The number of GAD67-positive perisomatic varicosities was normalized against the diameter of each presumed excitatory neuron. Histogram shows the plot of mean number of perisomatic boutons per cell (normalized to cell diameter, puncta/µm) in *Sert*$^{+/+}$ (n = 82) and *Sert*$^{-/-}$ (n = 91) neurons. (*C*) Top, example voltage clamp trace of mEPSCs recorded in excitatory LIV neurons of both *Sert*$^{+/+}$ and *Sert*$^{-/-}$ rats at V_h = −70 mV. Bottom, cumulative probability distributions and histograms of amplitude and frequency of mEPSCs in *Sert*$^{+/+}$ (n = 12) and *Sert*$^{-/-}$ (n = 11). (*D*) Top, example voltage clamp trace of mIPSCs recorded in excitatory LIV neurons of both *Sert*$^{+/+}$ and *Sert*$^{-/-}$ rats at V_h = +10 mV. Bottom, cumulative probability distributions and histograms of amplitude and frequency of mIPSCs in *Sert*$^{+/+}$ (n = 17) and *Sert*$^{-/-}$ rats (n = 16). (*E*) Left, example voltage clamp trace of evoked IPSCs onto LIV excitatory neurons within a barrel at different ISI (50, 100, 200, and 500 ms) at V_h = +10 mV in the presence of AMPA/NMDA blockers. Right, line plot depicting PPR Amp2/Amp1 at varying ISIs in *Sert*$^{+/+}$ (n = 8) and *Sert*$^{-/-}$ rats (n = 9). Data are represented as mean ± SEM, *P < 0.05 and ***P < 0.001 (*t*-test).

The lower frequency of mIPSCs recorded in *Sert*$^{-/-}$ LIV excitatory cells could be due to either a reduced number of inhibitory synapses onto LIV cells, supported by our finding of reduced number of perisomatic GAD67 puncta, and/or due to a diminished presynaptic probability of release of inhibitory vesicles. We tested the dynamic changes in presynaptic transmitter release by evoking inhibitory vesicle release in the vicinity of the recorded LIV excitatory neurons using a paired-pulse of varying ISI (50, 100, 200, and 500 ms). Because mIPSCs recorded onto LIV excitatory cells most abundantly originate

from local cortical inhibitory networks (Porter et al. 2001; Beierlein et al. 2003), IPSCs were evoked within the home barrel in the presence of AMPAR/NMDAR blockers. We detected no differences in the PPRs (Fig. 4E; $Sert^{+/+}$ $n = 8$; $Sert^{-/-}$ $n = 9$; 50 ms, $P = 0.90$; 100 ms, $P = 1.0$; 200 ms, $P = 0.12$; 500 ms, $P = 0.18$), indicating similar levels of release probability.

Depolarized GABA Reversal Potential Associated with Lower $GABA_A$ Receptor and KCC2 Transporter Expression within S1 of $Sert^{-/-}$ Rats

The depolarized E_{GABA} of LIV excitatory neurons as well as the smaller mIPSC amplitudes observed in $SERT^{-/-}$ rats demonstrate an altered driving force for GABA receptor-mediated ionic currents. In addition, the smaller mIPSC amplitudes could be caused by a downregulated expression of $GABA_A$ receptors. Furthermore, the alpha 1 (α1) subunit of GABA receptors has been shown to be located at parvalbumin-positive perisomatic synapses onto pyramidal cells, involved in FFI (Nusser et al. 1996; Freund and Katona 2007). To investigate possible changes in expression, we quantified the amount of $GABA_A$ receptor α1 and α2 subunits in total S1 protein extracts from somatosensory cortex tissue using western blot. We observed a 22% reduction in $GABA_A$ α1 receptor subunit expression in $Sert^{-/-}$ rats compared with $Sert^{+/+}$ rats (Fig. 5A; $Sert^{+/+}$ 1, $n = 4$; $Sert^{-/-}$ 0.78 ± 0.06, $n = 4$; $t(3) = 3.38$, $P < 0.05$) whereas $GABA_A$ α2 receptor subunit expression was comparable across the genotypes (Fig. 5B; $Sert^{+/+}$ 1, $n = 4$; $Sert^{-/-}$ 0.88 ± 0.08, $n = 4$; $t(3) = 1.39$, $P = 0.26$).

We further investigated the molecular mechanisms that could underlie the altered driving force of GABA receptor-mediated ion currents. Throughout development, a sequential expression of 2 chloride transporters, NKCC1 and KCC2, help to define the reversal potential for chloride, and therefore the drive for $GABA_A$ mediated inhibitory responses, being depolarizing in the early postnatal phase and shunting or more hyperpolarizing in the mature brain (Ben-ari et al. 2007). In this respect, an increase in NKCC1 or decrease in KCC2 could explain the observed depolarized inhibitory reversal potential. We therefore quantified the protein expression of both chloride transporters in somatosensory cortex tissue using western blot of total S1 cross-linked protein lysates to obtain a ratio of functional surface (S) to the internal (I) expression of chloride transporters of P21 $Sert^{+/+}$ and $Sert^{-/-}$ rats. We found no genotypic differences in terms of total protein expression and S/I ratios

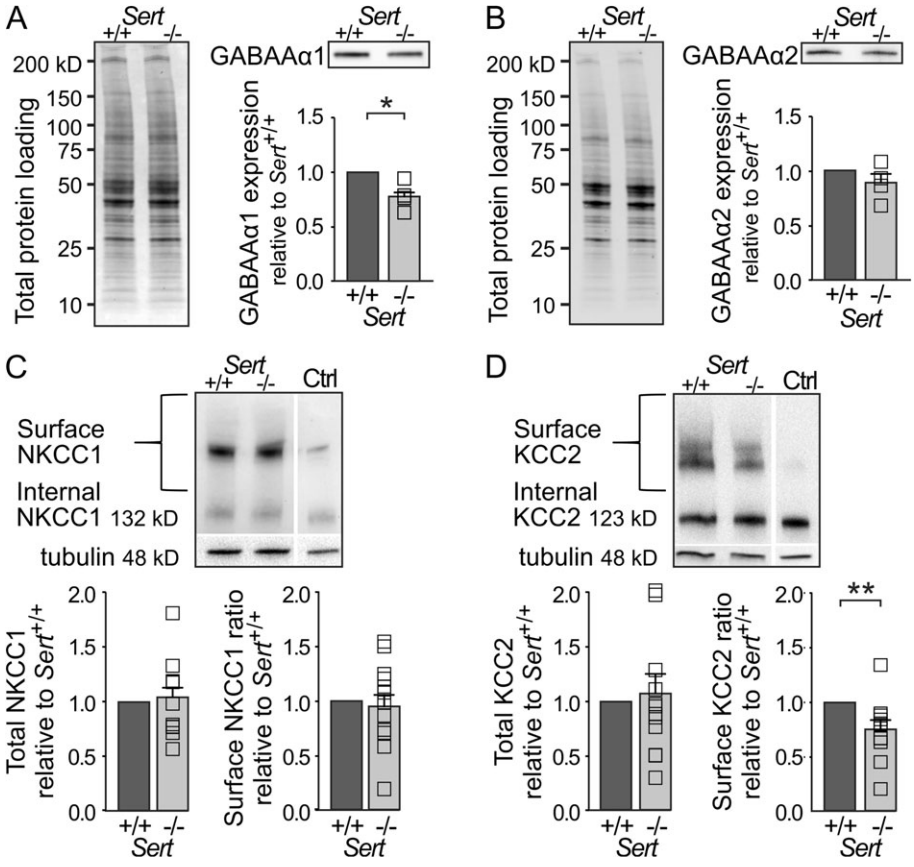

Figure 5. Reduced inhibitory drive in $Sert^{-/-}$ rats is associated with a decrease in GABAA α1 subunit expression as well as a reduced KCC2 chloride extruder protein expression within S1. (*A*) Western blot analysis of GABAA α1 subunit expression in S1 total protein lysates of $Sert^{+/+}$ ($n = 4$) and $Sert^{-/-}$ rats ($n = 4$). Left, loading control. Right, western blot and histogram showing total GABAA α1 receptor subunit expression normalized to $Sert^{+/+}$. (*B*) Western blot analysis of GABAA α2 receptor subunit expression in S1 total protein lysates of $Sert^{+/+}$ ($n = 4$) and $Sert^{-/-}$ rats ($n = 4$). Left, loading control. Right, western blot and histogram showing total GABAA α2 subunit expression normalized to $Sert^{+/+}$. (*C*) Left, surface and internal NKCC1 protein levels were determined by BS^3 cross-linking method using S1 protein lysates of $Sert^{+/+}$ and $Sert^{-/-}$ rats with non-crosslinked control (Ctrl). Right, histograms showing quantification of total NKCC1 expression normalized to γ-tubulin and surface NKCC1 expression normalized to internal expression in $Sert^{+/+}$ ($n = 12$) and $Sert^{-/-}$ ($n = 12$) rats. (*D*) Left, surface and internal KCC2 protein levels were determined by BS^3 cross-linking method using S1 protein lysates of $Sert^{+/+}$ and $Sert^{-/-}$ rats with non-crosslinked control (Ctrl). Right, histograms showing quantification of total KCC2 expression normalized to γ-tubulin and surface KCC2 expression normalized to internal expression in $Sert^{+/+}$ ($n = 12$) and $Sert^{-/-}$ rats ($n = 12$). All data are presented as mean ± SEM, $^*P < 0.05$ and $^{**}P < 0.01$ (t-test).

for NKCC1 (Fig. 5C; total: $Sert^{+/+}$ $n = 12$, $Sert^{-/-}$ $n = 12$; $Sert^{-/-}$ 1.05 ± 0.09; $t(11) = 0.53$, $P = 0.60$; S/I: $Sert^{-/-}$ 0.98 ± 0.11; $t(11) = 0.16$, $P = 0.87$). However, while the total expression of KCC2 showed no genotypic differences (Fig. 5D; $Sert^{+/+}$ 1, $n = 12$, $Sert^{-/-}$; $Sert^{-/-}$ = 1.07 ± 0.66, $n = 12$; $t(11) = 0.36$, $P = 0.72$), we found KCC2 S/I expression to be significantly reduced in $Sert^{-/-}$ rats (Fig. 5D; $Sert^{-/-}$ = 0.76 ± 0.09; $t(11) = 2.56$, $P < 0.05$), exhibiting a 24% decrease in surface expression.

Taken together, our data indicate a reduction in the number of functional inhibitory synapses targeting LIV excitatory neurons associated with a decrease in postsynaptic $GABA_A$ α1 receptor expression. Combined with the measured depolarized E_{GABA} and reduced surface expression of KCC2 chloride extruder, these results may directly explain the observed decrease in efficiency of inhibitory control within the LIV circuits of $Sert^{-/-}$ rats.

Increased Intracortical Signal Propagation and Accelerated Tactile Navigation during Object Localization in $Sert^{-/-}$ Rats

Our structural (synaptic), functional, and molecular findings show a strong reduction in inhibitory control within the FFI circuits of LIV, which could change how cortical circuits integrate sensory information coming from the periphery (Foeller et al. 2005; Celikel and Sakmann 2007). We tested intracortical excitatory signal propagation by recording LFPs in brain slices mounted on MEAs following standardized bipolar electrical stimulation (−1 V, 200 µs) of neuronal circuits in LIV (Fig. 6A). We compared the negative stimulus induced CNQX sensitive (i.e., AMPA receptor-mediated) synaptic component of layer and column-specific LFPs (Fig. 6B, see Material and Methods for details) between $Sert^{+/+}$ ($n = 20$) and $Sert^{-/-}$ rats ($n = 20$) in LIV, upper LII/III and LVb. Mapping the confidence levels for all excitatory LFP responses upon LIV stimulation across experiments revealed a widening of the horizontal spread of the excitatory responses into the neighboring cortical columns in $Sert^{-/-}$ as compared with $Sert^{+/+}$ (Supplementary Fig. 3). We furthermore found a general increase in the response amplitudes of the excitatory synaptic LFP component (Fig. 6C; $F(1,8) = 10.2$, $P < 0.0001$) in particular within the home column. There excitatory synaptic LFP amplitudes were increased by 87.9% within LIV ($Sert^{+/+}$ −141.6 ± 12.3 µV; $Sert^{-/-}$ −266.1 ± 20.4 µV; $t(8) = 10.5$, $P < 0.001$), and by 57.9% in the upper supragranular LII/III, $Sert^{+/+}$ −77.7 ± 9.0 µV; $Sert^{-/-}$ −122.7 ± 13.9 µV; $t(8) = 3.8$, $P < 0.01$). This implies that in the somatosensory cortex of $Sert^{-/-}$ rats, efferent excitatory signal propagation between LIV circuits and its projection target is generally increased.

To address the role of altered FFI in LIV in processing tactile information, we quantitatively studied the sensory information

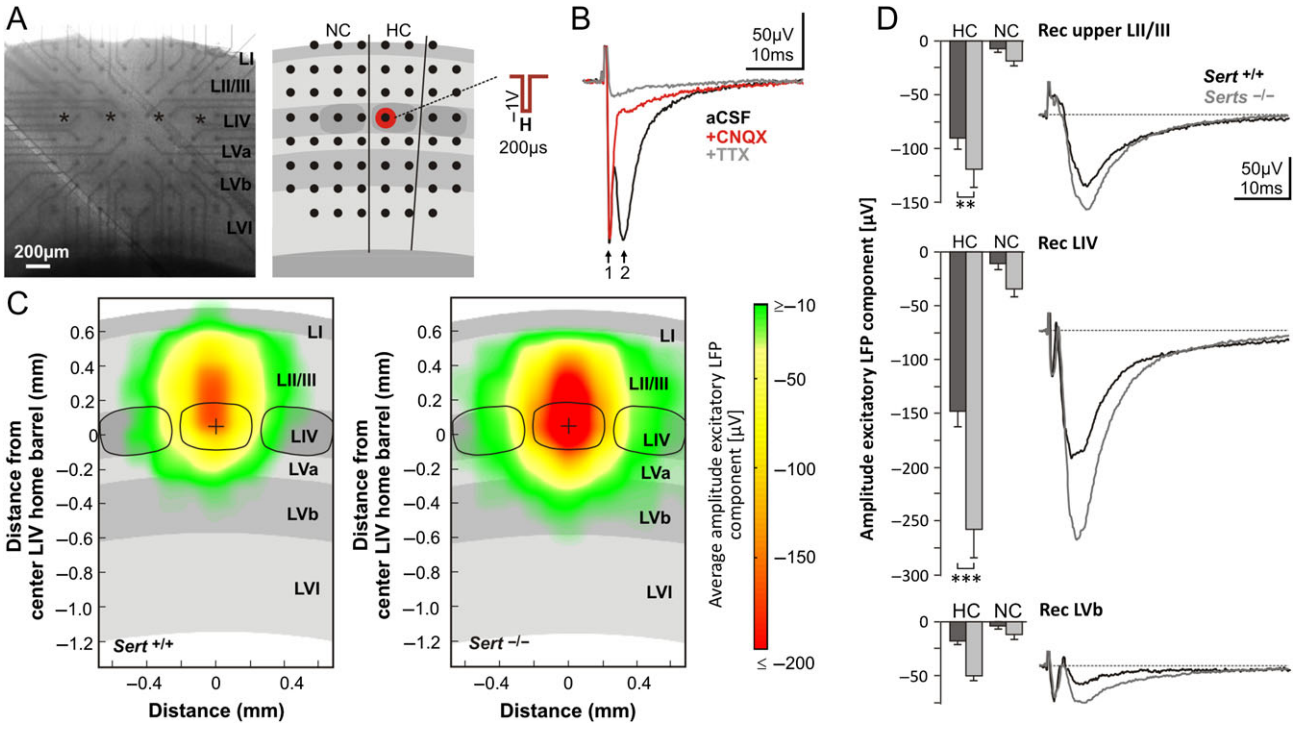

Figure 6. Intracortical excitatory signal propagation following activation of LIV networks is increased in $Sert^{-/-}$ rats. (*A*) Photograph of an acute brain slice mounted on a MEA chip and schematic representation of slice positioning relative to electrode positions (black dots). Electrical stimulation of LIV networks was applied by a block voltage pulse through a MEA electrode positioned in a LIV barrel (red dot). *HC*, (stimulated) home column; *NC*, neighboring column. (*B*) Pharmacological identification of main components of evoked LFPs. Representative LFP response in LIV first under 1) ACSF condition (black trace), showing a fast action potential volley (arrow 1) and a slow AMPA mediated synaptic component (arrow 2), 2) After 30 min under 5 µM CNQX (red trace) and 3) After 30 min under 5 µM CNQX + 1 µM TTX (gray trace). (*C*) Averaged maps of excitatory signal propagation, constructed by linearly transforming individual maps ($Sert^{+/+}$: $n = 15$; $Sert^{-/-}$: $n = 15$) to the cortical template shown as gray background centered to one LIV barrel center (black dot). The maps illustrate the averaged amplitude of excitatory synaptic LFP responses with confidence levels ≥68.3%. (*D*) Average negative (excitatory) synaptic peak amplitudes of LFPs following LIV stimulation for $Sert^{+/+}$ ($n = 20$) and $Sert^{-/-}$ rats ($n = 20$). Data were obtained from the electrode delivering the strongest LFP response in each of the 3 layers of interest (upper LII/III = second electrode row; LIV = fourth electrode row; LVb = sixth electrode row) separately for HC and NC. Traces show representative averaged LFP recordings at the respective laminar positions in the HC. Data are means ± SEM. Asterisks indicate significant differences between the 2 genotypes. Two-way ANOVA with Bonferroni correction was used. Data are represented as mean ± SEM, $^{**}P < 0.01$ and $^{***}P < 0.001$. See Supplementary Fig. 3 for maps of confidence levels of the excitatory response.

Sert$^{+/+}$ (n = 8) and *Sert*$^{-/-}$ (n = 8) juvenile rats require to perform a whisker dependent object localization task (Voigts et al. 2008, 2015). On this task, the so-called spontaneous gap-crossing task, animals are required to locate an elevated tactile target in darkness after they are positioned on an elevated (home) platform located at a distance from the target platform. Before each trial, the target was pseudorandomly positioned at "nose" or "whisker" distances where animals could collect tactile information using mechanoreceptors in the skin and/or with their whiskers (Fig. 7A). Tactile exploration of the target platform was observed using high-speed infrared imaging (Voigts et al. 2008; Pang et al. 2011; Juczewski et al. 2016) and tactile evidence (i.e., duration of whisker contact; Fig. 7B) before successful object localization was quantified using video recordings (see Materials and Methods; Fig. 7C). Rats of both genotypes were able to learn the task at comparable rates (Fig. 7D; Learning effect: F = 84.52; P < 0.001; Genotype effect: F = 0.22; P = 0.64, 2-way ANOVA with df = 1). However, analysis of the total duration of tactile exploration showed that *Sert*$^{-/-}$ rats made significantly less contacts compared with *Sert*$^{+/+}$ rats prior to successful object localization when the object was located at distances where the animals could reach it using only their whiskers (Fig. 7E; *Sert*$^{+/+}$ 1.06 s ± 0.17; *Sert*$^{-/-}$ 0.62 s ± 0.1; P = 0.042; t = 2.057; n = 59 and 51 trials, respectively). At shorter, "nose," distances the 2 groups were not significantly different despite the tendency for *Sert*$^{-/-}$ to require less tactile exploration (Fig. 7E; *Sert*$^{+/+}$ 0.83 ± 0.16; *Sert*$^{-/-}$ 0.55 ± 0.11; P = 0.19; t = 1.32; n = 60 and 39 trials, respectively). The latency between the first contact and the successful object localization was significantly shorter for *Sert*$^{-/-}$ rats when the target was located at whisker (Fig. 7F; *Sert*$^{+/+}$ 2.49 s ± 0.19; *Sert*$^{-/-}$ 1.77 ± 0.17; P < 0.01; t = 2.720; n = 59 and 51 trials, respectively) but not at nose distances (*Sert*$^{+/+}$ 2.39 ± 0.24; *Sert*$^{-/-}$ 2.37 ± 0.26; P = 0.966; t = 0.43; n = 60 and 39 trials, respectively), suggesting that *Sert*$^{-/-}$ rats not only required less tactile information to successfully locate the target, but also did so faster than *Sert*$^{+/+}$ rats (Fig. 7G) without altering the temporal distribution of tactile contacts with the target (Supplementary Fig. 4).

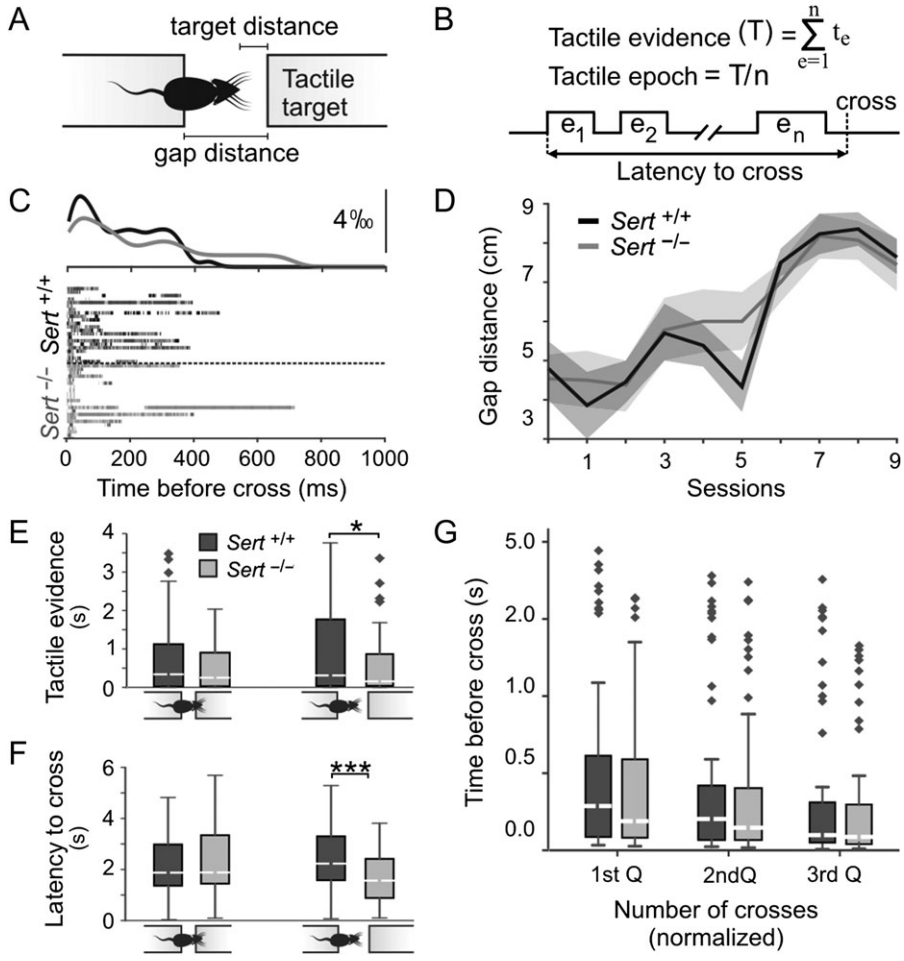

Figure 7. *Sert*$^{-/-}$ rats show faster decision-making during tactile object localization. (*A*) Cartoon representation of the behavioral task. (*B*) Schematic representation of temporal distribution of tactile exploration on a given trial and key independent parameters extracted for the quantification of tactile exploration. (*C*) Temporal distribution of whisker contacts onto target prior to successful object localization. Twenty-five randomly chosen trials at whisker distances in each genotype were plotted after aligning the trials at gap-cross. Peri-contact time histograms (top) were normalized to the sum of all contacts on each trial. (*D*) Learning curves described as the maximum distance animals could successfully locate the target across sessions (*Sert*$^{-/-}$ n = 8; *Sert*$^{+/+}$ n = 8 animals). (*E*) Histogram showing total duration of exploration prior to successful object localization when the object was located either at "nose" distances in *Sert*$^{+/+}$ (n = 60 trials) and *Sert*$^{-/-}$ (n = 39 trials) rats, or at "whisker" distance (*Sert*$^{+/+}$ n = 60; *Sert*$^{-/-}$ n = 51 trials). (*F*) Histogram showing the latency between the first contact and the successful object localization with target locations at nose distance in *Sert*$^{+/+}$ (n = 60 trials) and *Sert*$^{-/-}$ (n = 39 trials) rats, or at whisker distance (*Sert*$^{+/+}$ n = 60 trials; *Sert*$^{-/-}$ n = 51 trials). (*G*) Temporal distribution of whisker contacts was comparable across genotypes. Diamonds denote outliers *P < 0.05 and ***P < 0.001 (2-way ANOVA and t-test). See Supplementary Fig. 4 for temporal distribution of whisker contacts.

Discussion

We investigated whether increased extracellular 5-HT levels may affect the establishment of key networks for inhibitory control within primary somatosensory cortical networks and how this further impacts sensory integration using a model of SERT loss of function (*Sert*$^{-/-}$). Quantifying the feedforward inhibitory drive in the *Sert*$^{-/-}$ rat barrel cortex, we showed that elevating brain 5-HT levels during critical periods of development can be associated with reduced inhibitory control over TC recipient networks in cortical LIV of juvenile rats. At many levels, we find deficits in intracortical inhibitory circuitry within the *Sert*$^{-/-}$ genotype reflected by: 1) a reduction in GABA/AMPA ratio in LIV excitatory neurons, 2) fewer functional soma-targeting inhibitory synapses onto LIV excitatory neurons, 3) a decreased $GABA_A$ α1 receptor expression, 4) a depolarized E_{GABA} in excitatory LIV neurons and 5) a decrease in membrane KCC2 chloride extruder. On the level of the intracortical excitatory circuitry, we find a facilitation of the stimulus-evoked signal propagation in LII/III after LIV stimulation. Interestingly, when evaluating the ability of *Sert*$^{-/-}$ rats to detect the location of an object in space using their whiskers, we observe faster reaction times as well as fewer whisker contacts (i.e., less sensory exploration) required to successfully locate the platform.

The fine balance of excitatory and inhibitory cortical networks that mediate FFI is essential for gating incoming TC input, for effectively blocking recurrent excitation and preserving distinct signaling in cortical networks (Sun et al. 2006). We show that FFI is impaired in the *Sert*$^{-/-}$ rat, where the GABAergic disynaptic transmission onto LIV excitatory neurons, following thalamic stimulation is significantly reduced. This mechanism relies on the recruitment of soma targeting FS interneurons (Daw et al. 2007; Chittajallu and Isaac 2010) for effectively shunting latent incoming information. Our thalamic stimulation combined with single neuron recording imply that the excitatory TC drive of the FS LIV inhibitory neurons was reduced, whereas that of LIV excitatory neurons remained similar. However, due to the limitations of electrical mapping in isolating single TC afferents, direct observation of the thalamic input onto excitatory and inhibitory neurons are yet to be realized. Nonetheless, intracortically we found a strong reduction in soma-targeting inhibition onto *Sert*$^{-/-}$ LIV neurons. Furthermore, the observed reduction of GABA α1 receptor subunit expression suggests a reduction in perisomatic parvalbumin positive inhibitory synapses directly involved in FFI (Freund and Katona 2007). Together with the observed depolarized E_{GABA}, we show multiple levels of impaired inhibitory control which affect *Sert*$^{-/-}$ rats and directly impact the integration of somatosensory information within the input layer of S1.

FFI allows temporally correlated thalamic excitation to summate onto excitatory LIV neurons before engaging a strong inhibitory shunt for any latent information. It is hypothesized that a reduction in inhibitory control would therefore diminish spike-timing precision and result in a widening of the time window during which positive feedback can play a role in amplifying the excitatory response (Fox et al. 1996; Kyriazi et al. 1996; Puzerey and Galán 2014). Successful localization of an object in the environment requires the preservation of complex spatial and temporal information along intracortical somatosensory networks. With others, we have previously shown that the *Sert*$^{-/-}$ phenotype exhibits a disrupted topological organization of the barrel cortex (Cases et al. 1996; van Kleef et al. 2012; Miceli et al. 2013; Chen et al. 2015). Despite their altered topological organization we show here that *Sert*$^{-/-}$ rats still successfully integrate sensory information from the periphery, locating tactile targets of interest using solely whisker touch. Interestingly, increased excitability along the intracortical projections facilitates the integration of sensory information across whisk cycles such that *Sert*$^{-/-}$ rats required fewer whisker touch and showed faster response times compared *Sert*$^{+/+}$ rats. These results are in agreement with recent observations in a mouse of Fragile X syndrome (Juczewski et al. 2016) where hyperexcitability of the primary somatosensory neurons have been well characterized (Zhang et al. 2014; Juczewski et al. 2016). Collectively, the findings point to an inverse correlation between somatosensory cortical excitability and the duration of tactile sampling required for successful object localization by whisker contacts.

The function of thalamic clustering and overall topological organization of primary sensory cortices affect the spatio-temporal processing of incoming stimuli (DeAngelis et al. 1999). The barrelless (Brl) mouse, a spontaneous mutant which lacks AC1 is characterized by TC afferent overlap and the absence of visible barrels. Interestingly, the Brl mouse can still perform tactile sensory tasks and has also shown a shorter latency of LIV neuron activation following surround whisker activation (Welker et al. 1996). Single- and multi-whisker activation both lead to accurate decision-making on a sensory detection task, where multi-whisker exploration reduces the latency to decision without altering the probability of successful object localization (Hutson and Masterton 1986; Celikel and Sakmann 2007). These results corroborate our findings that *Sert*$^{-/-}$ rats showing a strong TC as well as LIV excitatory neuron axonal projection overlap (Miceli et al. 2013) require fewer sensory inputs for correct responses on the gap crossing task. Welker et al. (1996) have argued that the overlap of TC afferents generates a cortical neuronal receptive field that is more appropriate to a continuous and less discriminate representation of the tactile periphery (Welker et al. 1996). The gap crossing task embodies such a stimulus in that the detection of the presence of a platform does not require complex sensory discrimination abilities. This is in sharp contrast to a novel object discrimination task which would involve the ability to discriminate between intricate textures and topologies, which has recently been reported to be impaired in the *Sert*$^{-/-}$ rat (Kroeze et al. 2016). Previous studies have implied impaired tactile performance in Sert$^{-/-}$ mice (Pang et al. 2011) and postnatally fluoxetine (SERT inhibitor) exposed rats (Lee 2009). Whether the discrepancy arises from species differences or is based on the transient pharmacological intervention is currently unclear. Regarding our findings, we argue that the reduction in inhibitory control of LIV excitatory neurons combined with the broadened barrel organization (Miceli et al. 2013) and increased synaptic transmission from LIV to LII/III (in space and time) might serve as a compensatory mechanism to amplify and make sense of potentially weak and non-topologically organized, incoming peripheral signals. The broadening of the excitatory signal propagation into adjacent cortical columns in *Sert*$^{-/-}$ rats is in agreement with the reduced column-specific axonal projection patterns of LIV excitatory neurons (Miceli et al. 2013). Reasons for the increased strength of excitatory synaptic transmission observed for local LIV networks as well as between LIV and LII/III could theoretically be found in 1) increased numbers of activated excitatory LIV neurons, either due to increased neuronal densities or intrinsic excitability, or 2) due to increased numbers and more efficient excitatory synapses established by these LIV neurons. However, our

current results as well as that of a previous study (Miceli et al. 2013) argue against the latter interpretation. It should nevertheless be considered that although no significant change in the total number of $GABA^+$ neurons was found, inhibitory neurons have been found to show protracted postnatal maturation after the initial critical period in the second week and at the juvenile age (Le Magueresse and Monyer 2013). Thus, changes in cell distribution may appear in older *Sert*$^{-/-}$ animals. We furthermore cannot rule out possible alterations in cell numbers of particular classes of inhibitory neurons. Previous studies have shown that for example, the number of PV^+ neurons were reduced following sensory deprivation (Patz et al. 2004; Desgent and Ptito 2012). Thus, future studies focussing on inhibitory neuron subtype quantifications may demonstrate changes at that level as it has recently been shown in altered laminarization of VIP^+ expressing neurons in *Sert*$^{-/-}$ mice (Frazer et al. 2015). Furthermore, a possible explanation for the observed increased excitatory synaptic propagation in *Sert*$^{-/-}$ rats could be that upon stimulation of LIV networks which activate both excitatory and inhibitory neurons, the disinhibition prevents proper cut of the stimulation induced action potential firing of excitatory cells, and consequently results in increased local neuronal firing. Future in vivo electrophysiological as well as imaging studies will be important in evaluating and quantifying the total effect of this reduced inhibitory control on the excitatory response following whisker deflection. Complementary to that, functional assessment of the consequence of broadened axonal projections and receptive fields might benefit from studying tactile exploration during fine scale texture discrimination.

The maturation of functional excitatory and inhibitory circuits within sensory cortices depends on experience and relies on afferent neuronal activity to develop (Allen et al. 2003; Foeller et al. 2005; Hensch 2005; Jiao et al. 2006; Lee et al. 2007; Spiegel et al. 2014). We have previously shown that the input/output connectivity of *Sert*$^{-/-}$ rat resembles that of an immature cortex possessing extensive transcolumnar as well as infragranular axonal innervations (Miceli et al. 2013). Here, the fewer soma targeting inhibitory synapses onto excitatory LIV neurons observed in *Sert*$^{-/-}$ rats as well the depolarized E_{GABA} and lower KCC2 surface expression are all indicative of an immature system (Chattopadhyaya et al. 2004; Blaesse et al. 2006). The latter could result from lower incoming sensory synaptic activity during the first postnatal weeks, a time at which the thalamic to LIV barrel pathway matures and the somatotopic pattern forms (Erzurumlu and Gaspar 2012). During this critical period SERT is transiently found on growing thalamic afferents (for review see Schubert et al. 2015) where it regulates extracellular 5-HT levels and modulates activity at the TC synapse (Rhoades et al. 1994; Laurent et al. 2002). A disruption of SERT function during these critical time points results in excessive presynaptic 5-HT1B receptor activation leading to impaired glutamatergic release upon LIV barrel neurons (Laurent et al. 2002). Reduction in incoming sensory activity during this early critical period, as it can also be induced by sensory deprivation such as whisker trimming from birth, has been shown to reduce the number of inhibitory synapses (Micheva and Beaulieu 1995; Gainey et al. 2016) and thus delays inhibitory circuit formation. Similarly, visual deprivation has been shown to decrease mIPSC frequency as well as GAD67 puncta density onto pyramidal cells of primary visual cortex (Gao et al. 2014). We believe that the reduced glutamate release at the TC synapse, which results from overactivation of presynaptic 5-HT1B receptors during the first postnatal weeks of sensory experience results in the observed decrease in mIPSC frequency and amplitude as well as the depolarized E_{GABA}. In this respect, as genetic ablation of *Sert* in rats has also been associated with reduced gene expression of transcription factor Npas4, Brain-Derived Neurotrophic Factor (BDNF) and GABAergic markers in the prefrontal cortex during early development (Guidotti et al. 2012), it is possible that BDNF, regulated by Npas4, serves as an upstream force driving the differential development of cortical excitatory/inhibitory circuitry in *Sert*$^{-/-}$ rats (Hong et al. 2008; Spiegel et al. 2014).

A translational aspect of the present research concerns the use of Selective Serotonin Reuptake Inhibitors (SSRIs) by pregnant mothers, which can pass the placenta and block SERT function in the developing human fetal brain (Bonnin et al. 2011; van Kleef et al. 2012). Further research investigating the effects of SSRIs, and resulting increase in extracellular 5-HT levels would therefore be informative and could permit to specifically dissect the time points at which 5-HT influences the structure and function of the developing barrel cortex. It also remains to be investigated whether the alterations shown in this study at the juvenile age are having lasting effects on the maturation of inhibitory control and functioning of cortical networks in the adult brain, in particular when impairment of SERT function is induced only transiently during early development, for example, due to exposure to SSRIs.

Changes in developmental SERT signaling have been linked to differential sensitivity to features of environmental stimuli (Belsky et al. 2009). A high prevalence of the short (s), low expressing variant of the SERT polymorphic region (5-HTTLPR) occurs in human populations and has been related to the Sensory Processing Sensitivity (SPS) personality trait. Interestingly, 5-HTTLPR s-allele carriers as well as individuals scoring high on the Highly Sensitive Person scale (high SPS) show increased sensitivity to both the adverse and supportive features of environmental stimuli (Aron et al. 2012; Pluess and Boniwell 2015) and are at higher risk for depressive disorders (Liss et al. 2005). As proper integration of primary sensory information is crucial for developing reliable and accurate constructs of our environment, the reduced inhibitory control within the cortical input LIV in S1 of *Sert*$^{-/-}$ rats, as identified in the present study, may provide a lead toward understanding the role of 5-HT homeostasis and its contribution to SPS and related neurological diseases (Homberg et al. 2016).

Supplementary Material

Supplementary material are available at *Cerebral Cortex* online.

Funding

The Dutch Organization for Scientific Research (Brain & Cognition grant, #433-09-311 to J.R.H. and D.S., Open Competition Grant, #824-14-022 to T.C.); the European Commission (Horizon2020, #660328 to T.C.).

Notes

We thank Rembrandt Bakker for the multi electrode array analysis toolbox (MEAMEA). We also thank Anthonieke Middelman, Jos Dederen, Karin de Haas-Cremers, and Astrid Oudakker for excellent technical assistance. *Conflict of Interest*: None declared.

References

Agmon A, Connors BW. 1991. Thalamocortical responses of mouse somatosensory (Barrel) cortex in vitro. Neuroscience. 41:365–379.

Allen CB, Celikel T, Feldman DE. 2003. Long-term depression induced by sensory deprivation during cortical map plasticity in vivo. Nat Neurosci. 6:291–299.

Altamura C, Dell'Acqua ML, Moessner R, Murphy DL, Lesch KP, Persico AM. 2007. Altered neocortical cell density and layer thickness in serotonin transporter knockout mice: a quantitation study. Cereb Cortex. 17:1394–1401.

Aron EN, Aron A, Jagiellowicz J. 2012. Sensory processing sensitivity: a review in the light of the evolution of biological responsivity. Personal Soc Psychol Rev. 16:262–282.

Bakker R, Schubert D, Levels K, Bezgin G, Bojak I, Kötter R. 2009. Classification of cortical microcircuits based on microelectrode-array data from slices of rat barrel cortex. Neural Netw. 22:1159–1168.

Beierlein M, Gibson JR, Connors BW. 2003. Two dynamically distinct inhibitory networks in layer 4 of the neocortex. J Neurophysiol. 90:2987–3000.

Belsky J, Jonassaint C, Pluess M, Stanton M, Brummett B, Williams R. 2009. Vulnerability genes or plasticity genes? Mol Psychiatry. 14:746–754.

Ben-ari Y, Gaiarsa J, Tyzio R, Khazipov R. 2007. GABA : a pioneer transmitter that excites immature neurons and generates primitive oscillations. Physiol Rev. 1215–1284.

Blaesse P, Guillemin I, Schindler J, Schweizer M, Delpire E, Khiroug L, Friauf E, Nothwang HG. 2006. Oligomerization of KCC2 correlates with development of inhibitory neurotransmission. J Neurosci. 26:10407–10419.

Bonnin A, Goeden N, Chen K, Wilson ML, King J, Shih JC, Blakely RD, Deneris ES, Levitt P. 2011. A transient placental source of serotonin for the fetal forebrain. Nature. 472:347.

Bruno RM, Sakmann B. 2006. Cortex is driven by weak but synchronously active thalamocortical synapses. Science. 312: 1622–1627.

Cases O, Vitalis T, Seif I, De Maeyer E, Sotelo C, Gaspar P. 1996. Lack of barrels in the somatosensory cortex of monoamine oxidase A-deficient mice: role of a serotonin excess during the critical period. Neuron. 16:297–307.

Celikel T, Sakmann B. 2007. Sensory integration across space and in time for decision making in the somatosensory system of rodents. Proc Natl Acad Sci USA. 104:1395–1400.

Celikel T, Szostak VA, Feldman DE. 2004. Modulation of spike timing by sensory deprivation during induction of cortical map plasticity. Nat Neurosci. 7:534–541.

Chamma I, Chevy Q, Poncer JC, Lévi S. 2012. Role of the neuronal K-Cl co-transporter KCC2 in inhibitory and excitatory neurotransmission. Front Cell Neurosci. 6:5.

Chattopadhyaya B, Di Cristo G, Higashiyama H, Knott GW, Kuhlman SJ, Welker E, Huang ZJ. 2004. Experience and activity-dependent maturation of perisomatic GABAergic innervation in primary visual cortex during a postnatal critical period. J Neurosci. 24:9598–9611.

Chen X, Ye R, Gargus JJ, Blakely RD, Dobrenis K, Sze JY. 2015. Disruption of transient serotonin accumulation by non-serotonin-producing neurons impairs cortical map development. Cell Rep. 10:346–358.

Chittajallu R, Isaac JTR. 2010. Emergence of cortical inhibition by coordinated sensory-driven plasticity at distinct synaptic loci. Nat Neurosci. 13:1240–1248.

Cruikshank SJ, Lewis TJ, Connors BW. 2007. Synaptic basis for intense thalamocortical activation of feedforward inhibitory cells in neocortex. Nat Neurosci. 10:462–468.

Cruikshank SJ, Urabe H, Nurmikko AV, Connors BW. 2010. Pathway-specific feedforward circuits between thalamus and neocortex revealed by selective optical stimulation of axons. Neuron. 65:230–245.

Daw MI, Ashby MC, Isaac JTR. 2007. Coordinated developmental recruitment of latent fast spiking interneurons in layer IV barrel cortex. Nat Neurosci. 10:453–461.

DeAngelis GC, Ghose GM, Ohzawa I, Freeman RD. 1999. Functional micro-organization of primary visual cortex: receptive field analysis of nearby neurons. J Neurosci. 19: 4046–4064.

Desgent S, Ptito M. 2012. Cortical GABAergic interneurons in cross-modal plasticity following early blindness. Neural Plast. 2012:590725.

Devlin B, Cook EH, Coon H, Dawson G, Grigorenko EL, McMahon W, Minshew N, Pauls D, Smith M, Spence MA, et al. 2005. Autism and the serotonin transporter: the long and short of it. Mol Psychiatry. 10:1110–1116.

Erzurumlu RS, Gaspar P. 2012. Development and critical period plasticity of the barrel cortex. Eur J Neurosci. 35:1540–1553.

Feldmeyer D, Egger V, Lubke J, Sakmann B. 1999. Reliable synaptic connections between pairs of excitatory layer 4 neurones within a single "barrel" of developing rat somatosensory cortex. J Physiol. 521(Pt 1):169–190.

Foeller E, Celikel T, Feldman DE. 2005. Inhibitory sharpening of receptive fields contributes to whisker map plasticity in rat somatosensory cortex. J Neurophysiol. 94:4387–4400.

Fox K, Glazewski S, Chen CM, Silva A, Li X. 1996. Mechanisms underlying experience-dependent potentiation and depression of vibrissae responses in barrel cortex. J Physiol Paris. 90:263–269.

Frazer S, Otomo K, Dayer A. 2015. Early-life serotonin dysregulation affects the migration and positioning of cortical interneuron subtypes. Transl Psychiatry. 5:e644.

Freund TF, Katona I. 2007. Perisomatic inhibition. Neuron. 56: 33–42.

Gabernet L, Jadhav SP, Feldman DE, Carandini M, Scanziani M. 2005. Somatosensory integration controlled by dynamic thalamocortical feed-forward inhibition. Neuron. 48:315–327.

Gainey M a., Wolfe R, Pourzia O, Feldman DE. 2016. Whisker deprivation drives two phases of inhibitory synapse weakening in layer 4 of rat somatosensory cortex. PLoS One. 11: e0148227.

Gao M, Maynard KR, Chokshi V, Song L, Jacobs C, Wang H, Tran T, Martinowich XK, Lee H. 2014. Rebound potentiation of inhibition in juvenile visual cortex requires vision-induced BDNF expression. J Neurosci. 34:10770–10779.

Gaspar P, Cases O, Maroteaux L. 2003. The developmental role of serotonin: news from mouse molecular genetics. Nat Rev Neurosci. 4:1002–1012.

Guidotti G, Calabrese F, Auletta F, Olivier J, Racagni G, Homberg J, Riva MA. 2012. Developmental influence of the serotonin transporter on the expression of npas4 and GABAergic markers: modulation by antidepressant treatment. Neuropsychopharmacology. 37:746–758.

Hensch TK. 2005. Critical period plasticity in local cortical circuits. Nat Rev Neurosci. 6:877–888.

Higley MJ, Contreras D. 2003. Nonlinear integration of sensory responses in the rat barrel cortex: an intracellular study in vivo. J Neurosci. 23:10190–10200.

Homberg JR, Olivier JDA, Smits BMG, Mul JD, Mudde J, Verheul M, Nieuwenhuizen OFM, Cools AR, Ronken E, Cremers T, et al. 2007. Characterization of the serotonin transporter knockout rat: a selective change in the functioning of the serotonergic system. Neuroscience. 146:1662–1676.

Homberg JR, Schubert D, Asan E, Aron EN. 2016. Sensory processing sensitivity and serotonin gene variance: insights into mechanisms shaping environmental sensitivity. Neurosci Biobehav Rev. 71:472.

Hong EJ, McCord AE, Greenberg ME. 2008. A biological function for the neuronal activity-dependent component of Bdnf transcription in the development of cortical inhibition. Neuron. 60:610–624.

Huang ZJ. 2009. Activity-dependent development of inhibitory synapses and innervation pattern: role of GABA signalling and beyond. J Physiol. 587:1881–1888.

Huang ZJ, Di Cristo G, Ango F. 2007. Development of GABA innervation in the cerebral and cerebellar cortices. Nat Rev Neurosci. 8:673–686.

Hull C, Scanziani M. 2007. It's about time for thalamocortical circuits. Nat Neurosci. 10:400–402.

Hutson KA, Masterton RB. 1986. The sensory contribution of a single vibrissa's cortical barrel. J Neurophysiol. 56: 1196–1223.

Isaacson JS, Scanziani M. 2011. Review how inhibition shapes cortical activity. Neuron. 72:231–243.

Jiao Y, Zhang C, Yanagawa Y, Sun Q-Q. 2006. Major effects of sensory experiences on the neocortical inhibitory circuits. J Neurosci. 26:8691–8701.

Juczewski K, von Richthofen H, Bagni C, Celikel T, Fisone G, Krieger P. 2016. Somatosensory map expansion and altered processing of tactile inputs in a mouse model of fragile X syndrome. Neurobiol Dis. 96:201–215.

Kasri NN, Nakano-Kobayashi A, Malinow R, Li B, Van Aelst L. 2009. The Rho-linked mental retardation protein oligophrenin-1 controls synapse maturation and plasticity by stabilizing AMPA receptors. Genes Dev. 23:1289–1302.

Kilman V, van Rossum MCW, Turrigiano GG. 2002. Activity deprivation reduces miniature IPSC amplitude by decreasing the number of postsynaptic GABA(A) receptors clustered at neocortical synapses. J Neurosci. 22:1328–1337.

Kimura F, Itami C, Ikezoe K, Tamura H, Fujita I, Yanagawa Y, Obata K, Ohshima M. 2010. Fast activation of feedforward inhibitory neurons from thalamic input and its relevance to the regulation of spike sequences in the barrel cortex. J Physiol. 588:2769–2787.

Kroeze Y, Dirven B, Janssen S, Kröhnke M, Barte RM, Middelman A, van Bokhoven H, Zhou H, Homberg JR. 2016. Perinatal reduction of functional serotonin transporters results in developmental delay. Neuropharmacology. 109: 96–111.

Kyriazi HT, Carvell GE, Brumberg JC, Simons DJ. 1996. Quantitative effects of GABA and bicuculline methiodide on receptive field properties of neurons in real and simulated whisker barrels. J Neurophysiol. 75:547–560.

Land PW, Kandler K. 2002. Somatotopic organization of rat thalamocortical slices. J Neurosci Methods. 119:15–21.

Laurent A, Goaillard J-M, Cases O, Lebrand C, Gaspar P, Ropert N. 2002. Activity-dependent presynaptic effect of serotonin 1B receptors on the somatosensory thalamocortical transmission in neonatal mice. J Neurosci. 22:886–900.

Le Magueresse C, Monyer H. 2013. GABAergic interneurons shape the functional maturation of the cortex. Neuron. 77: 388–405.

Lebrand C, Cases O, Wehrlé R, Blakely RD, Edwards RH, Gaspar P. 1998. Transient developmental expression of monoamine transporters in the rodent forebrain. J Comp Neurol. 401: 506–524.

Lee L-J. 2009. Neonatal fluoxetine exposure affects the neuronal structure in the somatosensory cortex and somatosensory-related behaviors in adolescent rats. Neurotox Res. 15: 212–223.

Lee S-H, Land PW, Simons DJ. 2007. Layer- and cell-type-specific effects of neonatal whisker-trimming in adult rat barrel cortex. J Neurophysiol. 97:4380–4385.

Liss M, Timmel L, Baxley K, Killingsworth P. 2005. Sensory processing sensitivity and its relation to parental bonding, anxiety, and depression. Pers Individ Dif. 39:1429–1439.

Luhmann HJ, Prince DA. 1991. Postnatal maturation of the GABAergic system in rat neocortex. J Neurophysiol. 65: 247–263.

Marik S a, Yamahachi H, McManus JNJ, Szabo G, Gilbert CD. 2010. Axonal dynamics of excitatory and inhibitory neurons in somatosensory cortex. PLoS Biol. 8:e1000395.

Meyer F. 1994. Topographic distance and watershed lines. Signal Process. 38:113–125.

Meyer HS, Wimmer VC, Hemberger M, Bruno RM, de Kock CPJ, Frick A, Sakmann B, Helmstaedter M. 2010. Cell type-specific thalamic innervation in a column of rat vibrissal cortex. Cereb Cortex. 20:2287–2303.

Miceli S, Negwer M, Van Eijs F, Kalkhoven C, Van Lierop I, Homberg J, Schubert D. 2013. High serotonin levels during brain development alter the structural input-output connectivity of neural networks in the rat somatosensory layer IV. Front Cell Neurosci. 7:88.

Micheva KD, Beaulieu C. 1995. An anatomical substrate for experience-dependent plasticity of the rat barrel field cortex. Proc Natl Acad Sci USA. 92:11834–11838.

Miller KD. 2003. Understanding layer 4 of the cortical circuit: a model based on cat V1. Cereb Cortex. 13:73–82.

Miller KD, Pinto DJ, Simons DJ. 2001. Processing in layer 4 of the neocortical circuit: new insights from visual and somatosensory cortex. Curr Opin Neurobiol. 11:488–497.

Nusser Z, Sieghart W, Benke D, Fritschy JM, Somogyi P. 1996. Differential synaptic localization of two major gamma-aminobutyric acid type A receptor alpha subunits on hippocampal pyramidal cells. Proc Natl Acad Sci USA. 93: 11939–11944.

Otsu N. 1979. A threshold selection method from gray-level histograms. IEEE Trans Syst Man Cybern. 9:62–66.

Pang RD, Wang Z, Klosinski LP, Guo Y, Herman DH, Celikel T, Dong HW, Holschneider DP. 2011. Mapping functional brain activation using [14C]-iodoantipyrine in male serotonin transporter knockout mice. PLoS One. 6:e23869.

Patz S, Grabert J, Gorba T, Wirth MJ, Wahle P. 2004. Parvalbumin expression in visual cortical interneurons depends on neuronal activity and TrkB ligands during an early period of postnatal development. Cereb Cortex. 14:342–351.

Peng H, Ruan Z, Long F, Simpson JH, Myers EW. 2010. V3D enables real-time 3D visualization and quantitative analysis of large-scale biological image data sets. Nat Biotechnol. 28: 348–353.

Persico AM, Mengual E, Moessner R, Hall FS, Revay RS, Sora I, Arellano J, DeFelipe J, Gimenez-Amaya JM, Conciatori M, et al. 2001. Barrel pattern formation requires serotonin uptake by thalamocortical afferents, and not vesicular monoamine release. J Neurosci. 21:6862–6873.

Pinal CS, Tobin AJ. 1998. Uniqueness and redundancy in GABA production. Perspect Dev Neurobiol. 5:109–118.

Pluess M, Boniwell I. 2015. Sensory-processing sensitivity predicts treatment response to a school-based depression

prevention program: evidence of vantage sensitivity. Pers Individ Dif. 82:40–45.

Porter JT, Johnson CK, Agmon A. 2001. Diverse types of interneurons generate thalamus-evoked feedforward inhibition in the mouse barrel cortex. J Neurosci. 21:2699–2710.

Puzerey PA, Galán RF. 2014. On how correlations between excitatory and inhibitory synaptic inputs maximize the information rate of neuronal firing. Front Comput Neurosci. 8:59.

Rebsam A, Seif I, Gaspar P. 2002. Refinement of thalamocortical arbors and emergence of barrel domains in the primary somatosensory cortex: a study of normal and monoamine oxidase a knock-out mice. J Neurosci. 22:8541–8552.

Rhoades RW, Bennett-Clarke CA, Shi MY, Mooney RD. 1994. Effects of 5-HT on thalamocortical synaptic transmission in the developing rat. J Neurophysiol. 72:2438–2450.

Riccio O, Potter G, Walzer C, Vallet P, Szabó G, Vutskits L, Kiss JZ, Dayer AG. 2009. Excess of serotonin affects embryonic interneuron migration through activation of the serotonin receptor 6. Mol Psychiatry. 14:280–290.

Roux L, Buzsáki G. 2015. Tasks for inhibitory interneurons in intact brain circuits. Neuropharmacology. 88:10–23.

Salichon N, Gaspar P, Upton AL, Picaud S, Hanoun N, Hamon M, De Maeyer E, Murphy DL, Mossner R, Lesch KP, et al. 2001. Excessive activation of serotonin (5-HT) 1B receptors disrupts the formation of sensory maps in monoamine oxidase a and 5-ht transporter knock-out mice. J Neurosci. 21:884–896.

Schubert D, Kötter R, Zilles K, Luhmann HJ, Staiger JF. 2003. Cell type-specific circuits of cortical layer IV spiny neurons. J Neurosci. 23:2961–2970.

Schubert D, Nadif Kasri N, Celikel T, Homberg J. 2015. Impact of monoaminergic neuromodulators on the development of sensorimotor circuits. In: Krieger P, Groh A, editors. Sensorimotor integration in the whisker system. New York, NY: Springer New York. p. 243–273.

Shoykhet M, Land PW, Simons DJ. 2005. Whisker trimming begun at birth or on postnatal day 12 affects excitatory and inhibitory receptive fields of layer IV barrel neurons. J Neurophysiol. 94:3987–3995.

Smits BMG, Mudde JB, van de Belt J, Verheul M, Olivier J, Homberg J, Guryev V, Cools AR, Ellenbroek BA, Plasterk RH, et al. 2006. Generation of gene knockouts and mutant models in the laboratory rat by ENU-driven target-selected mutagenesis. Pharmacogenet Genomics. 16:159–169.

Spiegel I, Mardinly AR, Gabel HW, Bazinet JE, Couch CH, Tzeng CP, Harmin DA, Greenberg ME. 2014. Npas4 regulates excitatory-inhibitory balance within neural circuits through cell-type-specific gene programs. Cell. 157:1216–1229.

Staiger JF, Bojak I, Miceli S, Schubert D. 2015. A gradual depth-dependent change in connectivity features of supragranular pyramidal cells in rat barrel cortex. Brain Struct Funct. 220: 1317–1337.

Staiger JF, Flagmeyer I, Schubert D, Zilles K, Kötter R, Luhmann HJ. 2004. Functional diversity of layer IV spiny neurons in rat somatosensory cortex: quantitative morphology of electrophysiologically characterized and biocytin labeled cells. Cereb Cortex. 14:690–701.

Stevens CF. 2003. Neurotransmitter release at central synapses. Neuron. 40:381–388.

Sun Q-Q, Huguenard JR, Prince DA. 2006. Barrel cortex microcircuits: thalamocortical feedforward inhibition in spiny stellate cells is mediated by a small number of fast-spiking interneurons. J Neurosci. 26:1219–1230.

Swadlow HA. 2003. Fast-spike interneurons and feedforward inhibition in awake sensory neocortex. Cereb Cortex. 13:25–32.

van Kleef ESB, Gaspar P, Bonnin A. 2012. Insights into the complex influence of 5-HT signaling on thalamocortical axonal system development. Eur J Neurosci. 35:1563–1572.

Vincent L. 1993. Morphological grayscale reconstruction in image analysis: applications and efficient algorithms. IEEE Trans Image Process. 2:176–201.

Voigts J, Herman DH, Celikel T. 2015. Tactile object localization by anticipatory whisker motion. J Neurophysiol. 113:620–632.

Voigts J, Sakmann B, Celikel T. 2008. Unsupervised whisker tracking in unrestrained behaving animals. J Neurophysiol. 100:504–515.

Welker E, Armstrong-James M, Bronchti G, Ourednik W. 1996. Altered sensory processing in the somatosensory cortex of the mouse mutant barelless. Science. 271:1864–1867.

Wilent WB, Contreras D. 2005. Dynamics of excitation and inhibition underlying stimulus selectivity in rat somatosensory cortex. Nat Neurosci. 8:1364–1370.

Zhang Y, Bonnan A, Bony G, Ferezou I, Pietropaolo S, Ginger M, Sans N, Rossier J, Oostra B, LeMasson G, et al. 2014. Dendritic channelopathies contribute to neocortical and sensory hyperexcitability in Fmr1–/y mice. Nat Neurosci. 17:1701–1709.

Zhang Z, Jiao Y-Y, Sun Q-Q. 2011. Developmental maturation of excitation and inhibition balance in principal neurons across four layers of somatosensory cortex. Neuroscience. 174:10–25.

Zheng Y, Lin S, Kambhamettu C, Yu J, Kang SB. 2009. Single-image vignetting correction. IEEE Trans Pattern Anal Mach Intell. 31:2243–2256.